JOINT ADAPTIVE MODULATION AND CHANNEL CODING FOR WIRELESS MULTIMEDIA COMMUNICATIONS

A THESIS IN ELECTRICAL ENGINEERING

Presented to the faculty of the American University of Sharjah
College of Engineering
in partial fulfillment of
the requirements for the degree

MASTER OF SCIENCE

by
RIMAS ADNAN ZRAE
B.S. 2008

Sharjah, U.A.E
June 2011

JOINT ADAPTIVE MODULATION AND CHANNEL CODING FOR WIRELESS MULTIMEDIA COMMUNICATIONS

Rimas Adnan Zrae, Candidate for Master of Science in Electrical Engineering

American University of Sharjah, 2011

ABSTRACT

Wireless communication has witnessed a significant growth due to recent advances in technology. As a result, there has been a strong demand for various multimedia services and applications over wireless channels. Typically, multimedia data is large in volume with high bandwidth requirements; therefore multimedia communications over unreliable and bandwidth limited channels has been always a challenge. In addition, the compressed multimedia data is highly sensitive to information loss and channel bit errors. Transmission errors can cause decoding failure which will distort the reconstructed image or video. Forward error correction (FEC) techniques could be employed to reduce the effects of errors on the quality of the reconstructed multimedia information. However, these error correction schemes inflict redundant bits on the transmitted data resulting in a loss in the bandwidth efficiency. Thus, the challenge resides in protecting the compressed multimedia data to ensure reliable transmission against hostile channel conditions while having less impact on the bandwidth efficiency.

In this thesis, we outline a new approach to tackle the problem of reliable image and video transmission over wireless channels. We propose an adaptive transmission scheme that attempts to meet the available channel conditions through the

adaptation of the modulation modes and channel coding rates. The proposed scheme partitions the compressed image and video data into different bit streams with unequal importance as perceived by the human visual system. Then, it jointly considers the estimated channel conditions and the importance of the transmitted bit stream when deciding on the modulation mode and the coding rate. The proposed scheme attempts to meet a predefined target bit error rate (BER) and yet avoids over protection, hence it improves the bandwidth efficiency which consequently increases the effective transmission rate. The proposed scheme then decides on the transmission parameters which meet the predefined target BER using an *off-line* lookup table. This predefined BER is based on the sensitivity of the transmitted bit stream. The results show that image transmission over Rayleigh flat fading channel using the proposed adaptive modulation scheme achieves peak signal-to-noise ratio (PSNR) values slightly less than those of a fixed-modulation system resulting in an insignificant impact on the subjective quality of the reconstructed images. However, the spectral efficiency of the proposed scheme is improved up to 460%. Results also demonstrate that combining adaptive modulation and channel coding for image transmission provides a graceful trade-off between image quality and spectral efficiency. For video transmission, a modified version of the proposed scheme shows significant improvement in the spectral efficiency while maintaining an average PSNR value of 32 dB across the transmitted video frames with an acceptable perceptual quality and smooth playback. Furthermore, the overall performance of the proposed scheme degrades gracefully in the presence of imperfect channel estimation. In future work, the playback buffer occupancy could be considered along with the channel condition and the importance of the bit stream to reduce buffer starvation instants.

Contents

Abstract **iii**

List of Figures **vii**

List of Tables **ix**

Abbreviations **x**

Acknowledgments **xii**

1 Introduction **1**
1.1 Motivation and Challenges 3
1.2 Contribution and Outline 4

2 Background and Literature Review **7**
2.1 Overview of Still Image Coding: JPEG Standard 7
2.1.1 Baseline sequential mode compression 7
2.1.2 Coding of DC coefficients 10
2.1.3 Coding of AC coefficients 10
2.2 Overview of MPEG-4 PART 10: H.264/AVC 11
2.2.1 Slices and Slice Groups 11
2.2.2 Spatial Directional Intra Prediction Model 12
2.2.3 Motion Compensation Prediction Model 13
2.2.4 Entropy Coding 14
2.2.5 The JM Reference Software 14
2.3 Literature Review 15

3 Methodology **21**
3.1 System Model 21
3.1.1 Channel Model 22
3.1.2 Adaptive Modulation 23
3.1.3 Adaptive Forward Error Correction 26
3.1.4 Assumptions 32
3.2 Proposed Transmission Scheme 33
3.2.1 Image Transmission Using Adaptive Modulation Scheme . . . 35
3.2.2 Multimedia Transmission Using Joint Adaptive Modulation and Channel Coding Scheme 37

4 Performance Analysis **43**
4.1 Image Transmission Using Adaptive Modulation 43
4.1.1 Simulation Results 43
4.2 Image Transmission Using Joint Adaptive Modulation and Channel Coding 47
4.2.1 Simulation Results 47
4.3 Video Transmission Using Joint Adaptive Modulation and Channel Coding 51
4.3.1 Simulation Results 52
4.4 Sensitivity Evaluation 54

5 Conclusions and Future Work **57**

References **60**

Appendix **64**

A Huffman Tables for the DC and AC Coefficients of the JPEG Baseline Encoder **65**

Vita **71**

List of Figures

2.1 Block diagram of a baseline JPEG encoder. 8
2.2 Preparing of the DCT coefficients for entropy coding [22]. 10
2.3 Example of slice groups [23]. 12
2.4 Intraprediction in H.264/AVC [23]. 12
2.5 Illustration of macroblock partitioning into blocks of different sizes [20]. 13
2.6 Multireference picture prediction in H.264/AVC [23]. 14

3.1 System Model. 21
3.2 BER performance of BPSK, 4-QAM, 16-QAM and 64-QAM under flat Rayleigh fading conditions. 26
3.3 Convolutional Encoder [52]. 27
3.4 BER performance of convolutionally encoded BPSK, 4-QAM, 16-QAM and 64-QAM under flat Rayleigh fading conditions with $\mathcal{R}_C = 1/3$. . 30
3.5 BER performance of convolutionally encoded BPSK, 4-QAM, 16-QAM and 64-QAM under flat Rayleigh fading conditions with $\mathcal{R}_C = 1/2$. . 31
3.6 BER performance of convolutionally encoded BPSK, 4-QAM, 16-QAM and 64-QAM under flat Rayleigh fading conditions with $\mathcal{R}_C = 2/3$. . 31
3.7 BER performance of convolutionally encoded BPSK, 4-QAM, 16-QAM and 64-QAM under flat Rayleigh fading conditions with $\mathcal{R}_C = 3/4$. . 32
3.8 Algorithm to adapt the parameters of the purposed model. 34
3.9 Theoretical BER performance of BPSK, 4-QAM, 16-QAM and 64-QAM under flat Rayleigh fading conditions. 36
3.10 BER performance for various coded modulation schemes under flat Rayleigh fading conditions. 38
3.11 BER performance for various coded modulation schemes under flat Rayleigh fading conditions. 38
3.12 BER performance for various coded modulation schemes under flat Rayleigh fading conditions. 39

4.1 The average BER performance of the adaptive modulation scheme under flat Rayleigh fading conditions. 44
4.2 The average spectral efficiency of the adaptive modulation scheme under flat Rayleigh fading conditions. 44

4.3 Transmitted Lena image over Rayleigh fading channel using adaptive scheme. 45
4.4 The average PSNR performance of the adaptive modulation scheme under flat Rayleigh fading conditions. 46
4.5 The average BER performance of the adaptive modulation and channel coding scheme under flat Rayleigh fading conditions. 47
4.6 The average spectral efficiency of the adaptive modulation and channel coding scheme under flat Rayleigh fading conditions. 48
4.7 The average PSNR performances for Lena image using adaptive modulation and channel coding scheme under flat Rayleigh fading conditions. 49
4.8 Transmitted images over Rayleigh fading channel using adaptive modulation and channel coding scheme. 50
4.9 The average PSNR performances using adaptive modulation and channel coding scheme under flat Rayleigh fading conditions. 51
4.10 Snapshot of three video sequences using adaptive modulation and channel coding scheme under flat Rayleigh fading conditions. 52
4.11 The average PSNR performances of "Bus" video sequence using adaptive modulation and channel coding scheme under flat Rayleigh fading conditions. 53
4.12 The average spectral efficiency of "Bus" sequence using adaptive modulation and channel coding scheme under flat Rayleigh fading conditions. 54
4.13 The average BER performance of the adaptive modulation and channel coding scheme for target BER of 10^{-4} over Rayleigh fading channel. . 55
4.14 The average spectral efficiency of the adaptive modulation and channel coding scheme for target BER of 10^{-4} over Rayleigh fading channel. . 56

List of Tables

2.1 Luminance quantization table [21]. 9

3.1 Relationship between 2-bit information and the assigned phase for Gray encoding 23
3.2 The parameters of $\mathcal{R}_C = 1/3$ and $\mathcal{R}_C = 1/2$ convolutional codes [48]. 28
3.3 The parameters of $\mathcal{R}_C = 2/3$ and $\mathcal{R}_C = 3/4$ convolutional punctured codes [48]. 28
3.4 Convolutional codes information weight structure [53]. 30
3.5 Look-up table to achieve BERs of 10^{-5}, 10^{-4} and 10^{-3} using adaptive modulation. 37
3.6 Look-up table to achieve BERs of 10^{-3}, 10^{-4} and 10^{-5} using the adaptive modulation and channel coding scheme. 40
3.7 Comparison of PSNR results for JPEG algorithm 41

A.1 The category (CAT) of the baseline encoder [21]. 65
A.2 DC Huffman codewords of luminance [22]. 66
A.3 AC Huffman codewords of luminance [22]. 67

ABBREVIATIONS

ARQ	Automatic Repeat Request
AUEP	Adaptive Unequal Error Protection
AVC	Advanced Video Coding
AWGN	Additive White Gaussian Noise
BER	Bit Error Rate
BPSK	Binary Phase Shift Keying
CABAC	Context-Adaptive Binary Arithmetic Coding
CAVLC	Context-Adaptive Variable-Length Coding
CIF	Common Intermediate Format
CSI	Channel State Information
DCT	Discrete Cosine Transformation
DPCM	Differential Pulse Coding Modulation
ECC	Error Control Codes
FEC	Forward Error Correction
FMO	Flexible Macroblock Ordering
GOP	Group-of-Pictures

JPEG	Joint Photographic Experts Group
JSCC	Joint Source-Channel Coding
LC	Layered Coding
LOS	Line-of-Sight
MB	Macroblock
MDC	Multiple Description Coding
MIMO	Multiple-Input and Multiple-output
MPEG	Moving Picture Experts Group
PBDBS	Partial Backward Decodable Bit Stream
PDF	Probability Density Function
PSNR	Peak Signal-to-Noise Ratio
QAM	Quadrature Amplitude Modulation
QPSK	Quadrature Phase-Shift Keying
QoS	Quality of Service
RLE	Run Length Encoding
RVLC	Reversible Variable Length Coder
SNR	Signal-to-Noise Ratio
UEP	Unequal Error Protection
VLC	Variable Length Coding

Acknowledgments

My gratitude goes to my advisors Dr. Mohamed Hassan and Dr. Mohamed El-Tarhuni who supported me throughout my thesis with many valuable suggestions and helpful discussions while allowing me the room to work in my own way. This thesis would not have been possible without their guidance, encouragement and trenchant critiques. My appreciation must be extended to the College of Engineering for offering me a graduate teaching assistantship.

I wish to state the significant contribution of my mother who supported me throughout all stages of my life, and must have suffered a great deal of dedication to my study. In return to her everlasting care, support, encouragement and above all love, I present this effort with my deepest love and respect to her.

"*In loving memory of my Grandmother. If tears could build a stairway and memories were a lane, I would walk right up to heaven to bring you home again*"

Chapter 1

Introduction

Recently, wireless multimedia applications and services have undergone enormous development due to the significant and continuing growth of wireless communications. These applications demand reliable channels and high data rates. On the other hand, wireless channels are characterized by their limited bandwidth and time varying conditions. The challenge raised by the wireless communication lies in the contradiction between the limited bandwidth offered by the channel and the large volume of multimedia data as well as the strict quality of service (QoS) parameters (such as bit error rate (BER), delay and latency) required by multimedia applications. The wireless channel might also delay, lose, or corrupt individual packets. Losses have significant impact on the perceived quality due to spatiotemporal error propagation. Thus, to achieve the required high data rates and acceptable BER, the channel must be efficiently used to guarantee a maximum level of perceptual quality from the end-user's perspective.

Typically, video services are demanding applications in terms of bandwidth requirements, losses and delay bounds. Different video coding algorithms and standards have been introduced to enable smooth delivery of video services at an acceptable quality over time varying and bandwidth limited channels. Since most of these coding standards use lossy compression, the coded data stream becomes highly sensitive to information loss and channel bit errors resulting in severe distortion in the transmitted videos. Therefore an efficient video transmission scheme is always a goal that requires careful considerations.

The increasing demand for wireless multimedia transmission has motivated a

lot of researches on images and video communications over wireless systems. The implementation of joint source and channel coding schemes to transmit digital images and videos were investigated in [1], [2], [3], [4], [5], [6], [7]. Error resilience coding [8], [9], [10] and power allocation techniques [11], [12], [13] proved to enable reliable multimedia transmission over wireless channels. Error control methods [14], [15] and power control approaches [16], [17] are very effective strategies for supporting QoS in robust video transmission. Joint source coding and transmission power management [18], and joint power control and FEC [19] provide robustness against channel errors to minimize the amount of distortion in the received video sequence.

In this study, we address the application of joint adaptive modulation and channel coding and for multimedia transmission over wireless fading channels. We propose a new approach for selecting the appropriate modulation level and channel coding rate which jointly considers the perceptual quality and bandwidth efficiency. In this approach, the adaptation targets maximizing the bandwidth efficiency while maintaining high peak signal-to-noise ratio (PSNR) for an acceptable perceptual quality. In this work, we used JPEG algorithm for image compression. Since not all portions of the coded bitstream are equally important, our framework partitions the bitstream into sub-streams with different quality and protects each sub-stream based on its contribution to the final quality of the decompressed image. While for video compression we focused primarily on the H.264/AVC codec because of its high compression ratio and its error resilience. Through the data partitioning mode provided by H.264/AVC, the video stream is classified into different layers, each characterized by a different degree of importance in the decoding process. Thus, our transmission scheme allocates different protection levels to different portions of the video data based on their sensitivity to errors. An algorithm is developed and used to select the appropriate modulation mode and channel coding rate in order to efficiently protect the partitioned multimedia content against channel degradation. Simulation results show that adaptation according to the channel condition enhances the spectral efficiency and gives acceptable immunity against channel variations. While the

adaptation according to the sensitivity of the compressed multimedia content proved to prevent the channel from introducing unrecoverable errors and improve the quality of the reconstructed data.

1.1 Motivation and Challenges

The increasing demand for multimedia applications (e.g. HDTV, video conferencing, video telephony and video-on-demand), motivates the need for designing a robust and reliable transmission scheme over wireless channels.

A video stream consists of a sequence of still images (frames) displayed one after another to imitate motion and interactivity. Each of these images requires a large amount of storage and a fast and reliable channel for transmission. To reduce the amount of transmitted data, data compression techniques are needed. Typically, image and video compression algorithms achieve this by exploiting the inherent spatial and temporal redundancies. However, these algorithms are designed to remove spatial and temporal redundancies while assuming error free transmission. Hence, compressed video and image bit streams are highly sensitive to channel errors. This sensitivity is mostly because of the quantization and differential coding operations as well as the spatial and temporal interdependencies. The use of variable-length coding (VLC) in the erroneous compressed data would not allow even the non-corrupted parts to be correctly decoded until after the next synchronization point is obtained.

On the other hand, wireless channels are characterized by their limited bandwidth and time varying nature which poses other challenges on multimedia communications. Moreover, data transmission over wireless channels is susceptible to random bit errors due to a number of impairments, such as path loss, shadowing and multipath fading. Therefore, when a compressed bitstream is transmitted over such error-prone channels, the impact of bit errors might range from negligible, moderate, to extremely severe. Sometimes a single error could render a whole bit stream useless and might lead to the drop of the entire frame which typically degrades the quality

of the reconstructed information.

In multimedia communications, distortion in the reconstructed information can be classified into two types. The first type is the quantization distortion introduced by the lossy source encoding schemes and the second type is distortion due to channel errors. There are different ways to protect multimedia data against channel errors. Error control schemes at the highest level can be divided into two classes, namely, automatic repeat request (ARQ) and FEC. In ARQ schemes, a data block is encoded for error detection and when an error is detected at the receiver then retransmission is requested. Thus, these scheme are not suitable for time sensitive applications. The other viable option is employing FEC where a data block is encoded for error correction at the receiver without retransmission. However, FEC schemes add overhead data to provide the necessary correction capability. Clearly, this results a reduction in the effective data rate.

Another challenge is the time-sensitive nature of video information, where a video frame must be correctly received and decoded before its playback time. In addition, video frames exhibit interdependencies among themselves, whereby losing an important frame leads to the loss of the consecutive frames. Thus, any video transmission scheme has to provide sufficient robustness to handle these difficulties and ensure that the quality of the decoded video is not overly affected by the channel unreliability. Based on the previous discussion, the video quality could be improved by selecting the appropriate transmission parameters not only according to the channel conditions but also according to importance of the multimedia information.

1.2 Contribution and Outline

The contributions of this work are as follows:

- Develop an adaptive modulation scheme for wireless image transmission over Rayleigh flat-fading channels. Simulation results show significant improvement

in the spectral efficiency when compared to a fixed-modulation system, while maintaining an acceptable image quality.

- Develop an adaptive modulation and channel coding scheme for wireless image transmission over Rayleigh flat-fading channel. Simulation results demonstrate that such a collaborative adaptive modulation and channel coding provides efficient use of the wireless channel to enhance the bandwidth efficiency. It also shows that the proposed scheme provides an acceptable performance both subjectively and objectively of the transmitted images.

- Extend the proposed scheme to video transmission over wireless Rayleigh flat-fading channel. Simulation results show that a significant improvement in the spectral efficiency can be achieved while maintaining an acceptable PSNR values across the transmitted video frames with good perceptual quality and smooth playback.

The proposed transmission schemes differ from previous work in that they exploit the differential sensitivity of multimedia contents, where it adapts the modulation modes and channel coding rates based upon the relative importance that each portion has on the reconstructed images and videos to enhance the spectral efficiency while keeping an acceptable perceptual quality. Sensitivity evaluation was performed to assure the reliability and robustness of the developed transmission approach over wireless channels. Results show that the overall performance degrades gracefully in the presence of imperfect channel estimation. Although the proposed scheme was implemented for JPEG and H.264/AVC codecs, it can be extended to other similar coding schemes that use transform coding, motion compensation and entropy coding.

The rest of the thesis is organized as follows:

Chapter 2 provides a technical overview of JPEG and H.264/AVC coding standards and introduces a comprehensive review of the literature. In Chapter 3, we describe

the system model and explain the proposed adaptive transmission scheme. We will also look into the performance of various modulation modes and convolutional codes under flat Rayleigh fading conditions. In Chapter 4, the performance of the proposed scheme is evaluated through computer simulations. It demonstrates the impact on the bandwidth efficiency, BER performance, the objective and the subjective quality of the reconstructed images and videos. In Chapter 5, we draw the main conclusions and discuss the future work.

Chapter 2

Background and Literature Review

We addressed in Chapter 1 the challenges facing wireless multimedia transmission. There is a large amount of work in the literature that has been done to mitigate the impact of the transmission errors on the reconstructed data. In this chapter, we first introduce a technical overview of JPEG and H.264/AVC compression standards which is needed for a better understanding of both the literature review and the proposed methodology in Chapter 3. Then we provide a summary of the methods that have been developed and used for multimedia communications in the past few years.

2.1 Overview of Still Image Coding: JPEG Standard

Various coding schemes have been proposed for lossy data compression. The Joint Photographic Experts Group (JPEG) standard operates in three compression modes. These are called the baseline sequential mode, the progressive mode and the hierarchical mode. The baseline sequential process of the JPEG standard is used for image compression in this work.

2.1.1 Baseline sequential mode compression

In this mode, an image is partitioned into 8×8 non-overlapping pixel blocks from left to right and top to bottom. Each block is DCT coded to produce 64 coefficients (one DC and 63 AC coefficients). These coefficients are then quantized and entropy coded [20], [21], [22]. Figure 2.1 illustrates the JPEG's baseline compression algorithm.

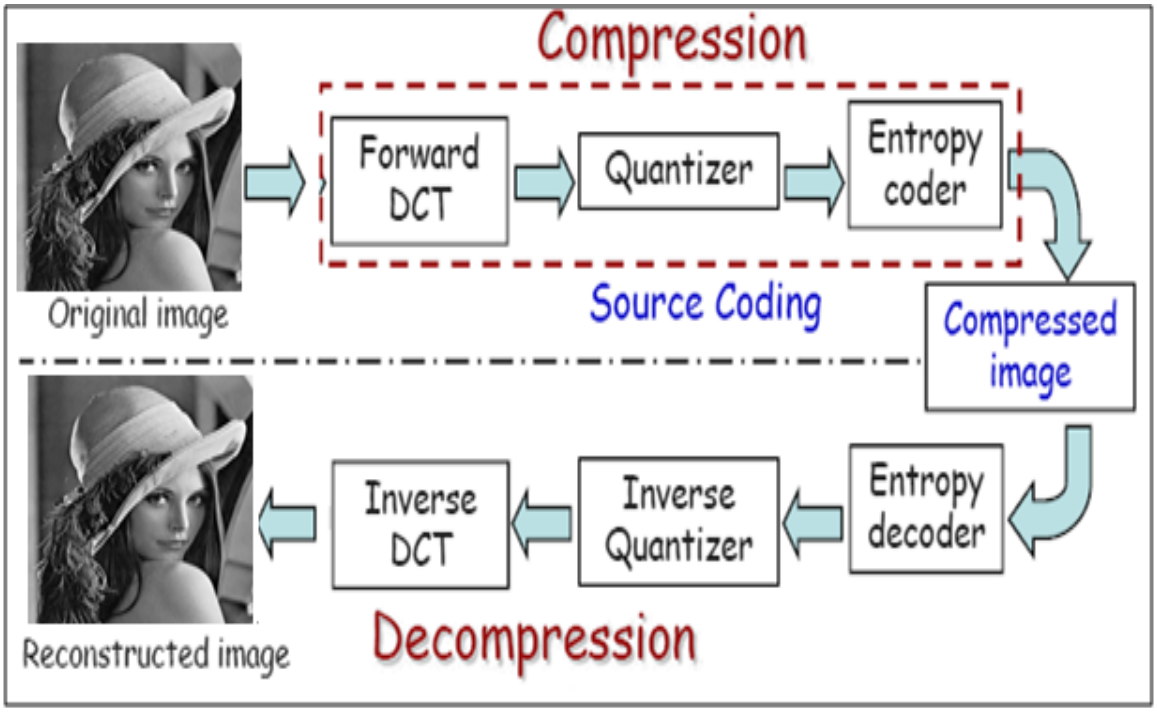

Figure 2.1: Block diagram of a baseline JPEG encoder.

The forward and inverse DCT are defined as follow:

FDCT:

$$S_{uv} = \frac{1}{4} C_u C_v \sum_{i=0}^{7} \sum_{i=0}^{7} S_{ij} \cos \frac{(2i+1)u\pi}{16} \cos \frac{(2j+1)v\pi}{16} \tag{2.1}$$

IDCT:

$$S_{ij} = \frac{1}{4} \sum_{i=0}^{7} \sum_{i=0}^{7} C_u C_v S_{uv} \cos \frac{(2i+1)u\pi}{16} \cos \frac{(2j+1)v\pi}{16} \tag{2.2}$$

$$C_u C_v = \begin{cases} \frac{1}{\sqrt{2}} & u, v = 0 \\ 1 & otherwise \end{cases}$$

where S_{ij} is the value of the pixel at position (i,j) in the block and S_{uv} is the trans-

formed (u,v) DCT coefficient. The 64 DCT coefficients are then quantized as follows:

$$S_{qyv} = \frac{S_{uv}}{Q_{uv}} \tag{2.3}$$

where S_{qyv} is quantized value of the DCT coefficient S_{uv}, and Q_{uv} is the quantization value obtained from the quantization table. The default quantization table was used in our model and is shown in Table 2.1.

16	11	10	16	24	40	51	61
12	12	14	19	26	58	60	55
14	13	16	24	40	57	69	56
14	17	22	29	51	87	80	62
18	22	37	56	68	109	103	77
24	35	55	64	81	104	113	92
49	64	78	87	103	121	120	101
72	92	95	98	112	100	103	99

Table 2.1: Luminance quantization table [21].

The dequantization at the decoder is performed as follows:

$$R_{qyv} = S_{quv} \times Q_{uv} \tag{2.4}$$

where R_{qyv} is the dequantized DCT value. After the quantization is done, the DC coefficient positioned at location (0,0) and the 63 AC coefficients are coded separately as shown in Figure 2.2. Differential pulse coding modulation (DPCM) is used to encode the DC coefficients to allow prediction of the DC coefficient from the previous block, i.e. $(DIFF = DC_i - DC_{i-1})$, as shown in Figure 2.2. Zigzag scanning is performed on the AC coefficients starting from the AC coefficient positioned at (1,0), then (0,1), etc.

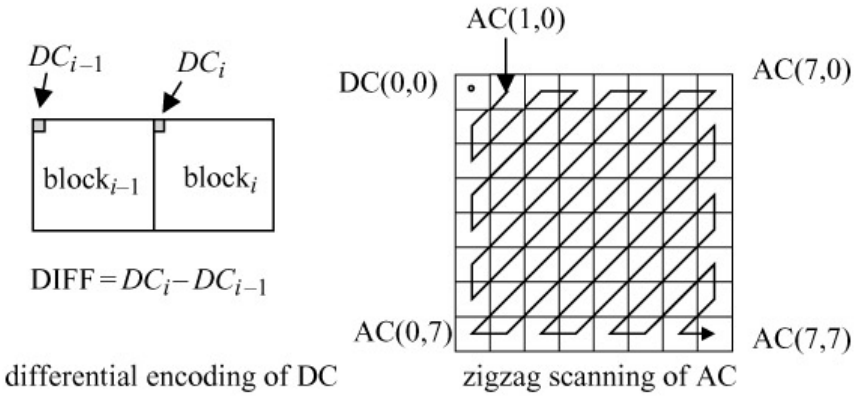

Figure 2.2: Preparing of the DCT coefficients for entropy coding [22].

In the following subsections we give more details on the process of the entropy coding of the DC and AC coefficients.

2.1.2 Coding of DC coefficients

All DC coefficients of each 8×8 block of the entire image are combined to make a sequence of combined coefficients. Only the first DC coefficient is encoded, followed by encoded differences of the other consecutive DC coefficients in the image. The DIFF values are categorized based on the magnitude range called category (CAT) as illustrated in Appendix A, Table A.1. Category zero is used for defining the end of block (EOB) code. Since the categories don't appear with the same frequency, they are variable length encoded as shown in Appendix A, Table A.2. VLC exploits this statistical property of the source by setting the shortest codewords to represent the most frequently occurring categories.

2.1.3 Coding of AC coefficients

After zigzag scanning, the resultant AC coefficients sequence will contain long zeroes strings within it. To exploit this feature, the AC coefficients are encoded using run-length encoding (RLE) and Huffman coding. Thus, more compression can be achieved by replacing long zeroes strings by short codewords. Each nonzero coefficient is

described by a (RUN, CAT) pair as shown in Appendix A, Table A.3. CAT represents the amplitude of a nonzero coefficient, and RUN is the number of zeros following that coefficient. An end of block (EOB) is assigned to indicate that the rest of the coefficients of the block are zeros.

2.2 Overview of MPEG-4 PART 10: H.264/AVC

In this section, we provide an overview of the H.264 or MPEG-4 Part 10 Advanced Video Coding (AVC). H.264/AVC is the most recent codec and it is designed to achieve the best quality at the highest compression ratio possible. It can deliver better video quality than previous codec at the same bit rate [20], [23], [24]. There are three profiles defined by H.264, namely, the baseline profile, the main profile, and the extended profile. The extended profile is used for video compression in this work, since it is intended for streaming applications. In the following subsections, we will introduce some features of H.264/AVC codec.

2.2.1 Slices and Slice Groups

Video frames are divided into macroblocks (MBs), each MB consists of a 16×16 luma pixels block, and two 8×8 chroma pixels blocks. Video frame can also be partitioned into slices, where a slice consists of an integer number of MBs. H.264/AVC supports flexible macroblock ordering (FMO) technique which allocates MBs into slice groups using a variety of slice mapping patterns. Each slice group contains several slices that are decoded independently. Hence, if one slice is lost the remaining slices can be reconstructed successfully. Figure 2.3 shows one way to allocate a MB within a video frame to one of three slice groups.

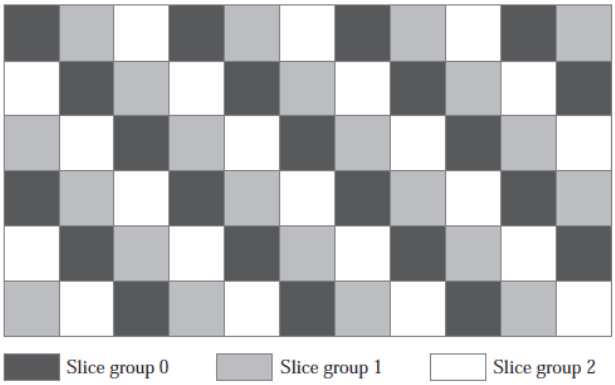

Figure 2.3: Example of slice groups [23].

2.2.2 Spatial Directional Intra Prediction Model

H.264/AVC provides spatial directional intra prediction model to predict a block of pixels from perilously decoded blocks. The supported intra prediction block sizes for the luma component are 4×4, 8×8 and 16×16. There are one DC and eight directional prediction modes enabled by H.264/AVC. For instance, in the horizontal prediction mode, the pixels to the left of the block are extrapolated horizontally as illustrated in Figure 2.4. In diagonal down-right prediction mode, each pixels are extrapolated at a 45° angle down to the right. When the 4×4 intra prediction block is chosen, each 4×4 luma block within a MB is allowed to use different prediction mode. The intra prediction for 8×8 block is formed similarly, while for the 16×16 block only four prediction modes are possible.

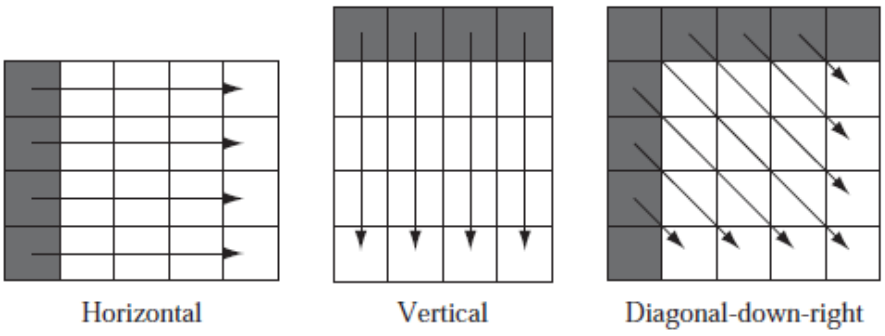

Figure 2.4: Intraprediction in H.264/AVC [23].

2.2.3 Motion Compensation Prediction Model

In motion compensation prediction, a MB in a previously reconstructed frame can be used for the prediction of a current MB through the transmission of motion vectors. H.264/AVC provides a powerful motion compensation model that includes variable block size for motion compensation and a multiple reference picture buffer. The inter-prediction process can be preformed with variable block sizes including 16×16, 16×8, 8×16, 8×8, 8×4, 4×8, and 4×4 as illustrated Figure 2.5.

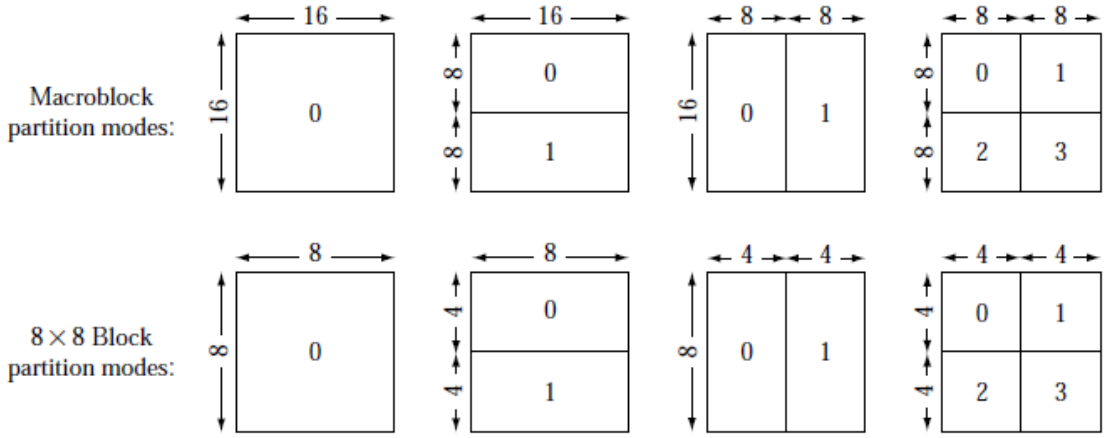

Figure 2.5: Illustration of macroblock partitioning into blocks of different sizes [20].

The multiple reference picture buffer may contain up to 16 reference frames. Thus, H.264/AVC provides flexibility in terms of which pictures can be used as references. In previous coding standards, the reference frames were limited to only two frames that can be used for motion compensation. Figure 2.6 shows that a reference frame in a predictive slice (P-slice) can be located subsequent to the current MB. It also shows that to predict a MB in a bidirectional slice (B-slice), the reference frames can be both located temporally previous or subsequent to the current frame. Furthermore, the encoder may chose the B-slices to be references for the prediction of other frames.

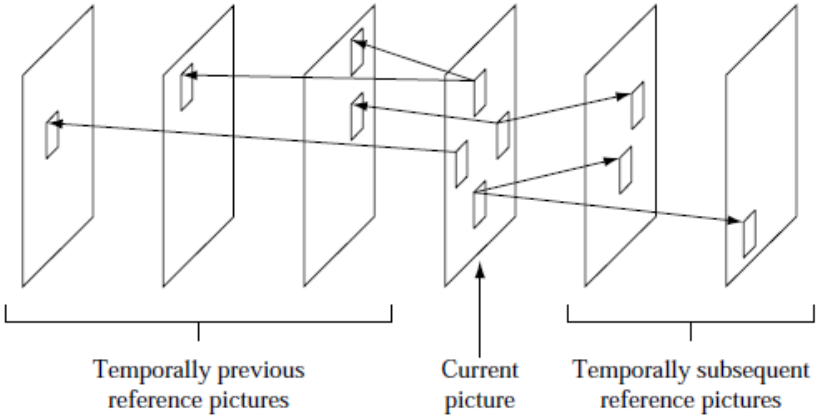

Figure 2.6: Multireference picture prediction in H.264/AVC [23].

2.2.4 Entropy Coding

There are two entropy coding methods specified in H.264/AVC. The simpler method is based on Context-Adaptive Variable-Length Coding (CAVLC) scheme. When CAVLC is used, the VLC tables are chosen based on statistical information like the number of non-zero coefficients in the neighboring blocks. The second method is based on Context-Adaptive Binary Arithmetic Coding (CABAC) scheme. In this method, non-binary symbols like the transformed coefficients and the motion vectors are converted to binary codes. These codes are further encoded using the arithmetic coder. CABAC method improves the compression ratio compared to CAVLC at the cost of higher computational complexity.

2.2.5 The JM Reference Software

The joint video team (JVT) developed the joint model (JM) reference software which is the implementation of the H.264/AVC as a **C** program [25]. The JM software encodes a video sequence in YUV format into an H.264 bitstream file and generates a trace file that records all the produced syntax elements of the coded video. At the decoder, the H.264 bitstream file is decoded into a video file which can be displayed using a YUV viewer.

2.3 Literature Review

In this section, we present a review of the literature on recent approaches towards multimedia communications over wireless channels.

The effects of adapting the source coding parameters to current communication conditions including energy, latency, quality of image, and bandwidth were investigated in [26]. The authors varied the scaling of the quantization values of JPEG image compression algorithm. While increasing the quantization level degrades the image quality, it reduces the number of bits to be transmitted as well as the required communication energy, latency, and bandwidth.

When images are transmitted over wireless channels they suffer from two types of source distortion. The first type is caused when transform coefficients are quantized and the second is caused by packet losses due to transmission errors. Distortion due to quantization can be controlled by the adaptive source coding while distortion due to packet losses can be reduced by joint source and channel coding. Joint Source-channel coding (JSCC) was considered in [1], [3], [5], [6], [7], [27], [28]. JSCC was introduced to reduce distortion, complexity, and delay in [7]. In integrated JSCC, the entropy coder and quantizer at the source coder, FEC and the modulation modes at the channel coder are jointly designed [28]. In image and video transmission, a compressed data shows different error sensitivities for different bit locations within the same frame. The UEP protects more the important bits of the frame than less important bits. While in adaptive FEC, the strength of protection depends on the state of the wireless link [5]. The JSCC scheme can improve image and video quality significantly when compared with schemes employing source rate control and/or channel code rate control unjointly.

However, JSCC schemes have few limitations. For instance, because of entropy coding, when a bit error occurs in the coded bit stream, it will propagate within the stream. The exact contribution of a bit error to the overall distortion is difficult to be estimated at the time of the encoding and most of the above-mentioned JSCC

techniques do not take into account entropy coding. A distortion model for the transmission of progressive JPEG compressed images over Rayleigh fading channels was proposed in [4] to predict quantization and channel errors. The prediction takes into account the channel bit error probability, the source coding rate and consider the effects of entropy coding and DPCM. Based on the same idea, the work was extended to MPEG-4 video in [2], [29] taking into account important aspects of video compression such as variable length coding, transform coding and motion compensation.

Error control codes (ECC) help to combat the channel errors however; traditional error control methods such as FEC or ARQ, are normally implemented at the expense of sacrificing transmission bandwidth. Hence, the key for robust and fast wireless multimedia transmission lies in increasing channel reliability and error resiliency without sacrificing the spectral efficiency [30]. The authors in [31] achieved considerable gain in terms of PSNR by exploiting the progressive source coding of JPEG2000 images to protect different portions of the data stream with different channel code rates. The code rates were chosen based upon the relative importance that each portion has on the reconstructed image.

The authors in [32] proposed a scheme to protect the coded bitstream by exploiting the multi-resolution structure of resolution-scalable coded stream and protects different resolution levels based on their sensitivity to channel errors. The proposed transmission strategy for scalable images and videos in [32] assigns the code rates based on the impact of channel errors at different resolution levels to enable considerable gains in terms of subjective and objective qualities.

An error detection and correction algorithm for H.263 coded video was suggested in [33] to improve the perceptual quality after the reception of the erroneous coded bitstream. The proposed error detection technique exploits the inherent redundancies within and outside MB to detect erroneously decoded MBs. The redundancies are measured in terms of a set of parameters based on MB and inner-DCT block similarities. For each MB, parameters are compared with thresholds to detect erroneous MBs. The information about each MB, whether erroneous or not, along with the

received bit stream are then used in a step-by-step decoding based correction.

In [34], the bandwidth efficiency degradation associated with channel coding was minimized by using UEP to protect scalable bitstreams against bit corruptions. The authors in [35] proposed an UEP scheme which jointly considers the temporal dependency of the frames in a group-of-pictures (GOP) and the quality dependency of the scalable layers in each frame. In more details, unequal amounts of protection were allocated to the different frames (I or P-frame) within a GOP, and in each frame, unequal amounts of protection were allocated to the progressive bitstream of the scalable video to provide a graceful degradation of video quality as packet loss rate varies.

Adaptive unequal error protection (AUEP) and VLC reshuffling techniques were applied in [36] to improve the resilience of image bitstreams when transmitted over wireless channels. Removal of a certain number of high frequency DCT coefficients in each MB was performed according to the current channel characteristics, allowing the application of a stronger channel code to the transmitted bits. The VLC reshuffling is used for reordering the important VLCs to the beginning of each MB. Due to VLC of entropy coding, a single bit error may result in a loss of synchronization and significant changes in the decoded symbol. One of the characteristics of the multimedia data stream is that it can be decoded even if it encounters transmission errors as long as the affected bits are restricted to certain limits.

Error-resilient tools can be classified into three major types, resynchronization, data recovery, and error concealment. These tools detect and locate errors, support fast resynchronization, and prevent the loss of entire information. Resynchronization tools attempt to establish the synchronization between the decoder and the incoming bitstream. They localize the error and prevent it from affecting the entire bitstream. Once synchronization is established, the data between the synchronization point prior to the errors and the first point where synchronization is reestablished are generally discarded. An effective resynchronization tool makes error recovery and concealment easier. After synchronization is reestablished, data recovery tools attempt to recover

the lost data as much as possible. How much data recovery can be achieved depends on the underlying coding scheme. For example, when a variable length coder is used, nothing can be done and hence the data between the two synchronization points before and after a detected error are discarded. However, when a reversible length coder (RVLC) is used [9], some amount of data can be recovered. In this approach, the variable length code words are designed such that they can be read in both forward and reverse directions. It provides a significant gain in objective and subjective visual quality. The performance of an error concealment strategy depends on the resynchronization scheme and its ability to effectively localize the error. The authors in [37] implemented a partial backward decodable bit stream (PBDBS) method, which is similar to RVLC, for H.263+ video transmission. This technique reverses the bit stream of some coded MBs so that these coded MBs can be decoded in a backward direction. When a decoder loses resynchronization, it searches the next resynchronization marker and decode the bitstream backwardly.

Error resilience techniques at the source coding level have been proved very helpful to enable reliable transmission of multimedia data over noisy/fading channels. The error resilient coding requires modifying the structure of the compressed bit stream. Data streams of image compression schemes can endure significant bit errors when error resilient mechanisms are applied [10]. At the decoder end, to further mitigate the effects of error, error concealment can always be applied.

Channel adaptive resource assignments techniques help to achieve the capacity of wireless communication systems. Energy efficiency is another important design consideration in wireless multimedia communications. Alleviating the effect of fading on the quality of signal transmission over wireless channels can be achieved through adaptive transmission rate and power assignment [11], [12], [18]. The mechanism of power control used in [38] measures the quality of the channel at the receiver to allow the transmitter to adjust the amount of transmitted power accordingly. Less power is allocated when the channel is in a good state while if the channel is in a bad state then more power is allocated. Another class of solutions could be applied by sending

more data when the channel is in a good state, while when the channel is a bad state less or no data should be transmitted. Schemes in this category can be classified as opportunistic schemes.

The quality of image transmission can be improved through the joint optimization of bit energy and channel coding. Minimizing the mean square error, or equivalently maximizing the PSNR, will decide the amount of bit energy and whether coding is used or not. The authors in [39] developed a rate-distortion transmission power adaptation scheme for video streaming over wireless channels. The scheme extracts feature variables from the video data, which describe its scene activity level. Based on these feature variables, the authors classified the video into a number of packet sets. For each set, the transmission distortion model developed in [40] and [41] is used to map the BER into the transmission distortion. Optimum allocation of the transmission power is then performed to minimize the overall transmission distortion. The power allocation methods have certain limitations such as using energy-distortion curves or simulations to predict the distortion. Constructing energy-distortion curves and/or running simulations increase the computational complexity of the optimization. However, it is not necessary that the channel will remain constant during the transmission of the packet, so if the channel changes during the transmission that would result in some quality degradation.

To increase the system capacity and reliability over wireless channels, multiple-input and multiple-output (MIMO) systems can be used [13]. In MIMO systems, multimedia coding techniques divide the coded data into different bitstreams with unequal importance that are transmitted using different antennas with different power levels. Improved quality and higher data rates without any overhead on total bandwidth were achieved. The transmitted power is kept constant during the symbol period and the effects of channel time-varying condition during the frame transmission were taken into consideration.

Another approach to enhance the quality of multimedia data transmission over wireless channels is through layered and multiple description coding [42], [43].

An image is divided into a number of layers in layered coding (LC) with different importance, namely, base layer and enhancement layers. To achieve the best picture quality, all layers should be correctly received. However, an acceptable approximation of the original image is guaranteed, when the base layer is received correctly while the enhancement layers are used to enhance the base layer quality. Thus, the more enhancement layers that are correctly received, the higher the quality of the reconstructed image. The simplest layering consists of two-layer coding, one base layer and one enhancement layer, where the low frequency components of the image are placed in the base layer while the high frequency information is placed in the enhancement layer. The level of protection increases as the importance of data increases. In multiple descriptions coding (MDC), an image is divided into layers of equal importance. A basic level of the reconstructed quality is guaranteed for each description alone. The quality can be enhanced more for additionally correctly received descriptions.

After this literature review, the proposed methodology will be explained in the next chapter.

Chapter 3

Methodology

In this study, we propose an efficient scheme for multimedia transmission over Rayleigh fading channels. For this aim, we investigate the performance of joint adaptive modulation and channel coding techniques while taking into consideration the importance of the bitstream and channel conditions. This is done to improve the spectral efficiency while keeping high PSNR performance for images and acceptable perceptual quality with smooth playback for videos.

3.1 System Model

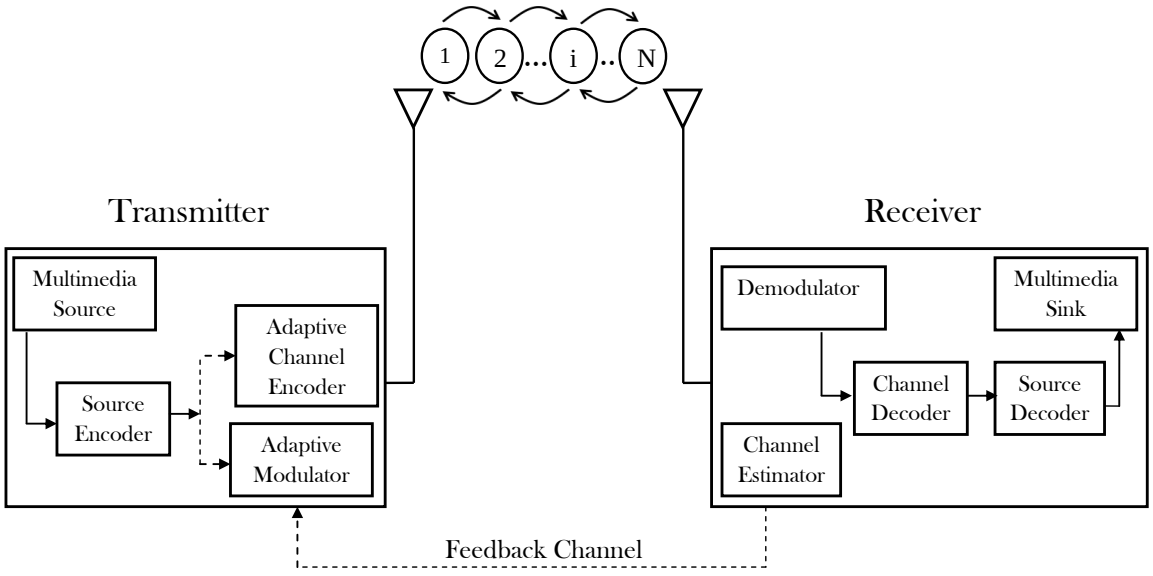

Figure 3.1: System Model.

Figure 3.1 depicts the block diagram of the proposed end-to-end transmission scheme. The digital images generated by the multimedia source are encoded using JPEG

compression algorithm while the videos are encoded using H.264/AVC standard as explained in Chapter 2. The output of the source encoder is then divided into different quality bitstreams with unequal importance. Accordingly, the bitstreams will be treated differently during transmission. The compressed data will be transmitted over a wireless channel using joint adaptive modulation and channel coding. We consider multi-state channel which has N states $\{1, 2, \ldots, N\}$. The received bitstream will be demodulated then decoded to reconstruct the images and videos. We assume that the channel state information (CSI) is available at the transmitter via reliable feedback channel[1].

In the following subsections, we describe the different blocks that compose the system model. After that, the proposed scheme will be explained in details.

3.1.1 Channel Model

In this thesis, we assume that the channel has a Rayleigh fading model. The Rayleigh distribution is used to model multipath fading channel with no direct line-of-sight (LOS) path. The channel fading amplitude α is a random variable with mean square value $\bar{\alpha^2} = \Omega$, and distributed according to [46]:

$$P_\alpha(\alpha) = \frac{2\alpha}{\Omega} exp\left(\frac{-\alpha^2}{\Omega}\right), \qquad \alpha \geqslant 0. \tag{3.1}$$

The probability density function (PDF) of the received SNR for Rayleigh fading is exponentially distributed as follows [47]:

$$P_\gamma = \frac{1}{\bar{\gamma}} exp\left(\frac{\gamma}{\bar{\gamma}}\right), \tag{3.2}$$

where γ is the instantaneous SNR and $\bar{\gamma}$ is the average SNR value.

[1]Channel estimation is beyond the scope of this thesis, we refer the interested reader to [44], [45] and the references therein.

3.1.2 Adaptive Modulation

In the proposed transmission scheme, adaptive modulation is used to take full advantage of the time-varying nature of wireless channels. In more details, the proposed model varies the data rate (constellation size) according to the channel condition to enhance the bandwidth (BW) efficiency. Several modulation levels are investigated in this study including BPSK, 4-QAM 16-QAM and 64-QAM.

3.1.2.1 BPSK/QPSK With Coherent Detection

The binary phase shift keying (BPSK) and quadrature phase-shift keying (QPSK) modulated signal can be expressed as [47]:

$$S(t) = \mathbf{A}_c \cos(2\pi f_c t + \theta_D(t)). \tag{3.3}$$

where $\mathbf{A}_c$ is the amplitude of the modulated signal, f_c is the carrier frequency and θ_D is the carries phase. For BPSK, $\theta_D(t) = 0$ when the source bit is 1 and $\theta_D(t) = \pi$ when the source bit is 0. While for QPSK, the relationship between the 2-bit information and the assigned phase is shown in Table 3.1.

Table 3.1: Relationship between 2-bit information and the assigned phase for Gray encoding

2-Bit information	$\theta_D(t)$
00	$-3\pi/4$
01	$3\pi/4$
10	$-\pi/4$
11	$\pi/4$

The probability of bit error for BPSK modulated signal in (AWGN) channel with no

fading is given by [48]:

$$P_b = Q\left(\sqrt{\frac{2E_b}{N_0}}\right), \tag{3.4}$$

while for QPSK, the bit error probability is:

$$P_b = 2Q\left(\sqrt{\frac{2E_b}{N_0}}\right) - Q^2\left(\sqrt{\frac{2E_b}{N_0}}\right). \tag{3.5}$$

where E_b/N_0 is the SNR per bit (energy per bit-to-noise power spectral density) and $Q(.)$ is the $Q-$function defined as:

$$Q(x) = \int_x^\infty \frac{1}{\sqrt{2\pi}} exp\left(\frac{-y^2}{2}\right) dy. \tag{3.6}$$

In the presence of fading, the received carrier amplitude $\mathbf{A}_c$, is attenuated by the fading amplitude α, while the received instantaneous signal power is attenuated by α^2. Thus, the instantaneous SNR per bit is $\gamma \triangleq \alpha^2 E_b/N_0$ and the average SNR per bit is $\bar{\gamma} \triangleq \bar{\alpha^2} E_b/N_0$. The probability of bit error of a BPSK modulated signal when transmitted over a Rayleigh fading channel is given by [46]:

$$P_b(\gamma) = \frac{1}{2}\left(1 - \sqrt{\frac{\bar{\gamma}}{1+\bar{\gamma}}}\right). \tag{3.7}$$

In the case of QPSK, a symbol includes 2 bits. Therefore, when the energy per bit is γ, then the energy per symbol $\gamma_s = 2\gamma$. When Gray encoding is applied, one symbol error result in only 1 bit error. Therefore, the BER for QPSK with coherent detection is given by [47]:

$$P_b^{QPSK} \backsimeq P_b^{BPSK},$$

$$P_b^{QPSK} \backsimeq \frac{1}{2}\left(1 - \sqrt{\frac{\bar{\gamma}}{1+\bar{\gamma}}}\right). \tag{3.8}$$

3.1.2.2 M-QAM With Coherent Detection

Quadrature amplitude modulation (QAM) can be viewed as a combined amplitude and phase modulation. Let M denote the number of possible transmitted waveforms, then in the n^{th} symbol interval the M-QAM signal can be expressed as [46]:

$$S(t) = \mathbf{A}_c(a_{In} + ja_{Qn}) \cos(2\pi f_c t + \theta_c). \tag{3.9}$$

where $\mathbf{A}_c$ is the amplitude of the modulated signal, f_c is the carrier frequency, θ_c is the carries phase, the in-phase and quadrature amplitudes a_{In} and a_{Qn} range over the values $\alpha_i = 2i - 1 - \sqrt{M}$, where $i = 1, 2, \ldots, \sqrt{M}$.

The probability of bit error for M-QAM systems with a square constellation in AWGN channel is [48]:

$$P_b = 4\left(1 - \frac{1}{\sqrt{M}}\right) Q\left(\sqrt{\frac{3\log_2 M}{M-1}\frac{E_b}{N_0}}\right) \times \left(1 - \left(1 - \frac{1}{\sqrt{M}}\right) Q\left(\sqrt{\frac{3\log_2 M}{M-1}\frac{E_b}{N_0}}\right)\right). \tag{3.10}$$

Thus, the BERs for 16-QAM and 64-QAM modulated signals respectively, are:

$$P_b^{16-QAM} = 3Q\left(\sqrt{\frac{4}{5}\frac{E_b}{N_0}}\right) \times \left[1 - \frac{3}{4}Q\left(\sqrt{\frac{4}{5}\frac{E_b}{N_0}}\right)\right]. \tag{3.11}$$

$$P_b^{64-QAM} = 3.5Q\left(\sqrt{\frac{2}{7}\frac{E_b}{N_0}}\right) \times \left[1 - \frac{7}{8}Q\left(\sqrt{\frac{2}{7}\frac{E_b}{N_0}}\right)\right]. \tag{3.12}$$

When an M-QAM signal is transmitted over a Rayleigh fading channel, the BER for each modulation is given by [47]:

$$P_b^{16-QAM} = \frac{3}{8}\left(1 - \frac{1}{\sqrt{1 + 5/2\bar{\gamma}}}\right). \tag{3.13}$$

$$P_b^{64-QAM} = \frac{7}{24}\left(1 - \frac{1}{\sqrt{1 + 7/\bar{\gamma}}}\right). \tag{3.14}$$

3.1.2.3 Numerical Results for Coherent Detection

Figure 3.2 shows the BER performance of Gray-encoded BPSK, QPSK (4-QAM), 16-QAM and 64-QAM under flat Rayleigh fading conditions.

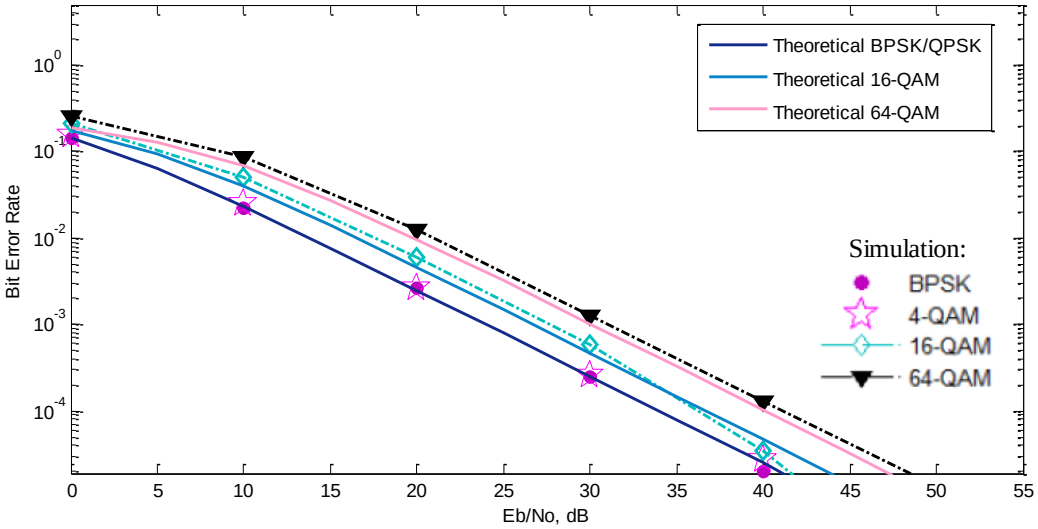

Figure 3.2: BER performance of BPSK, 4-QAM, 16-QAM and 64-QAM under flat Rayleigh fading conditions.

3.1.3 Adaptive Forward Error Correction

FEC schemes help to achieve reliable communications over wireless channels through the addition of redundant (parity) bits to detect and correct transmission errors. Thus, error detection and correction techniques result in additional overhead. However, when retransmission is not possible, FEC can improve the quality of the decoded data [47]. In the following section, we give a short discussion of convolutional coding since they are widely used in practice and will be used in our research.

3.1.3.1 Convolutional Coding

Convolutional coding is a powerful channel coding scheme for wireless mobile communication systems [49]. The convolutional encoder consists of **K**-shift registers and

modulo-2 adders connected to some of the stages as shown in Figure 3.3. The shift register consists of k-bit stages and n-linear algebraic function generators. A convolutional code is generated by passing the information sequence through the shift register k bits at a time, which transforms the k-input sequence into n-bits output channel code sequence. The code sequence is a new sequence that has redundancy in it. The rate at which the transmission is performed by the encoder is defined as the code rate, $\mathcal{R}_C$, where $\mathcal{R}_C = k/n$ and $\mathcal{R}_C \leqslant 1$. $\mathcal{R}_C$ and the constraint length ($\mathbf{K}$) determine the performance of the convolutional codes.

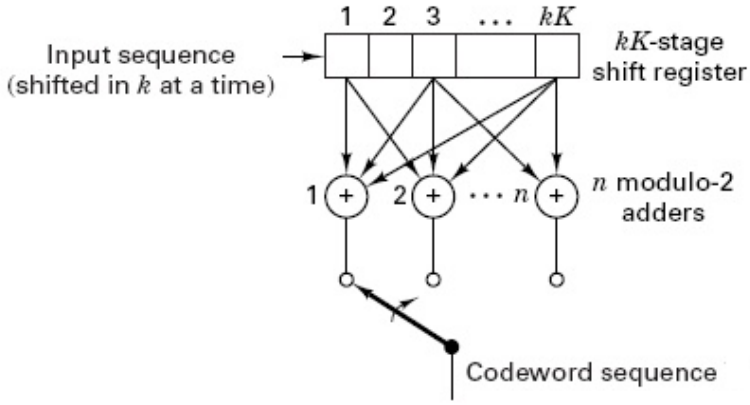

Figure 3.3: Convolutional Encoder [52].

The generator polynomials determine the error correction capability of the convolutional codes. Each code has its unique properties that are determined by the chosen polynomials. Another important parameter is the free distance (d_{free}) which is the minimum Hamming distance between different encoded sequences. Table 3.2 shows the optimum generator polynomials ($\mathbf{G}$) for $\mathcal{R}_C \in [1/3, 1/2]$. It also lists the upper bound on the free distance (d_{free}) of the convolutional code that can be achieved by the specified generators.

Table 3.2: The parameters of $\mathcal{R}_C = 1/3$ and $\mathcal{R}_C = 1/2$ convolutional codes [48].

Constraint length **K**	$\mathcal{R}_C$	$\mathbf{G}_1$	$\mathbf{G}_2$	$\mathbf{G}_3$	Upper Bound on d_{free}
3	1/3	110	111	111	8
3	1/2	110	111	-	5

High-rate $(n-1)/n$ punctured convolutional code can be generated from a low rate $1/n$ code in which some of the coded bits are deleted (punctured) from transmission. Punctured code reduces the free distance of the rate $1/n$ code by some amount that depends on the degree of puncturing. Table 3.3 shows the puncturing matrices ($\mathbf{P}$) for code rates 2/3 and 3/4 from the mother code $\mathcal{R}_C = 1/2$.

Table 3.3: The parameters of $\mathcal{R}_C = 2/3$ and $\mathcal{R}_C = 3/4$ convolutional punctured codes [48].

Constraint length **K**	$\mathcal{R}_C$	**P**	Upper Bound on d_{free}
3	2/3	10 11	3
3	3/4	101 110	3

Transmission errors convert a given code sequence $\boldsymbol{c}$ into the received sequence S_r. Maximum likelihood decoding compares the conditional probabilities $P(S_r/\grave{c})$ that the received sequence S_r corresponds to a possible code sequence $\grave{c}$, then decides on the sequence with the highest conditional probability [50]:

$$P(S_r/\grave{c}) = \max_{all\ \boldsymbol{c}} P(S_r/\boldsymbol{c}). \tag{3.15}$$

For any $\mathcal{R}_C = k/n$ convolutional code, the probability of bit error is upper bounded

by [51]:

$$P_b < \frac{1}{k} \sum_{d=d_{free}}^{\infty} B_d P_d, \tag{3.16}$$

where B_d is the total number of ones in the information bit on all weight (d) paths, and P_d is the probability of selecting a weight (d) output sequence as the transmitted code sequence while the weight zero sequence was actually sent. P_d is determined by the type of modulation and the channel model. This probability is given by:

$$P_d = [2\sqrt{p(1-p)}]^d. \tag{3.17}$$

where p is the probability of channel bit error. Since the average transmitted power is the same whether coded or uncoded bits are transmitted, then the average energy per coded bit is less than the average energy per uncoded bit. Thus, the probability of coded bit error is given by the P_d appropriate to the modulation type with the substitution:

$$\bar{\gamma_c} = \mathcal{R}_C \times \bar{\gamma}. \tag{3.18}$$

where $\bar{\gamma_C}$ is the SNR per bit for coded data bit. Hence, For BPSK/QPSK in Rayleigh fading channel, we get from (3.7) and (3.18):

$$p = \frac{1}{2}\left(1 - \sqrt{\frac{\mathcal{R}_C\bar{\gamma}}{1+\mathcal{R}_C\bar{\gamma}}}\right). \tag{3.19}$$

While for 16-QAM and 64-QAM respectively, we get from (3.13), (3.14) and (3.18):

$$p = \frac{3}{8}\left(1 - \frac{1}{\sqrt{1+5/2\mathcal{R}_C\bar{\gamma}}}\right), \tag{3.20}$$

$$p = \frac{7}{24}\left(1 - \frac{1}{\sqrt{1+7/\mathcal{R}_C\bar{\gamma}}}\right). \tag{3.21}$$

Table 3.4 lists the value of B_d for the convolutional codes we used in this study. Due to the fact that (3.16) converges rapidly, its common to use the first five to eight

terms.

Table 3.4: Convolutional codes information weight structure [53].

$\mathcal{R}_C$	$B_{d_{free}}$	$B_{d_{free+1}}$	$B_{d_{free+2}}$	$B_{d_{free+3}}$	$B_{d_{free+4}}$	$B_{d_{free+5}}$	$B_{d_{free+6}}$	$B_{d_{free+7}}$
1/3	3	0	15	0	58	0	201	0
1/2	1	4	12	32	80	192	448	1024
2/3	1	10	45	226	853	-	-	-
3/4	15	104	540	2520	11048	-	-	-

3.1.3.2 Numerical Results for BER Performance of Convolutional Code Under Flat Rayleigh Fading Conditions

To validate our results, Figures 3.4, 3.5, 3.6 and 3.7 show the BER performance as a function of channel SNR for coded BPSK, QPSK, 16-QAM and 64-QAM respectively, in flat Rayleigh fading channel.

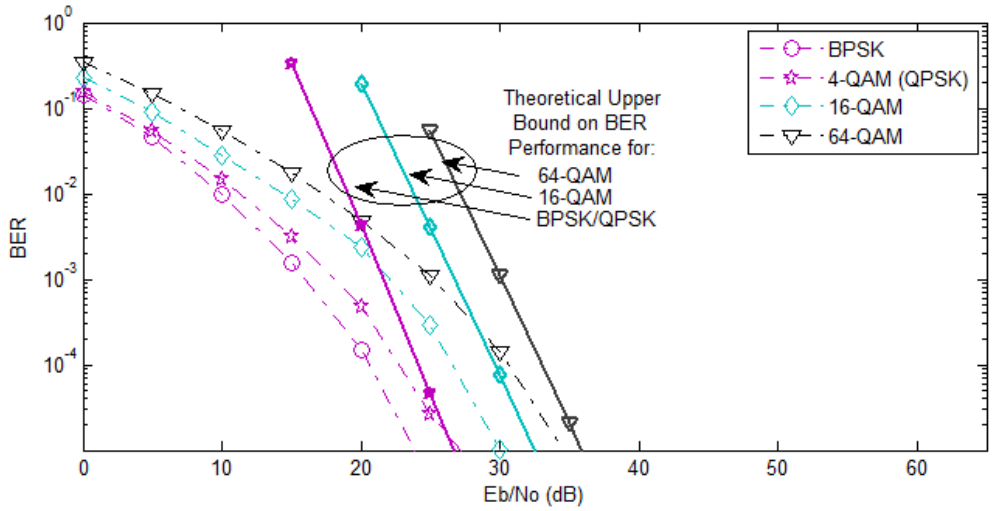

Figure 3.4: BER performance of convolutionally encoded BPSK, 4-QAM, 16-QAM and 64-QAM under flat Rayleigh fading conditions with $\mathcal{R}_C = 1/3$.

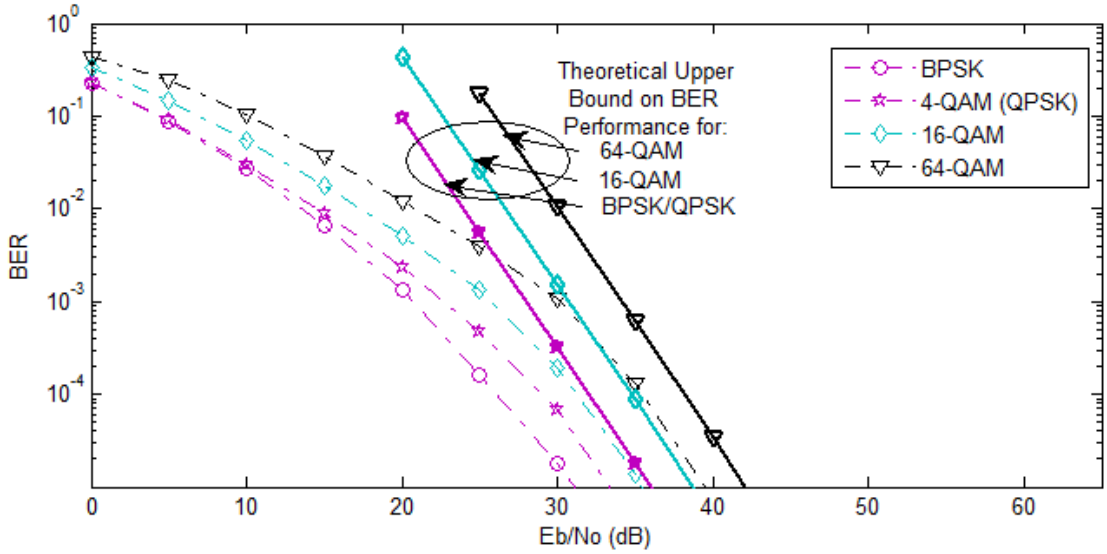

Figure 3.5: BER performance of convolutionally encoded BPSK, 4-QAM, 16-QAM and 64-QAM under flat Rayleigh fading conditions with $\mathcal{R}_C = 1/2$.

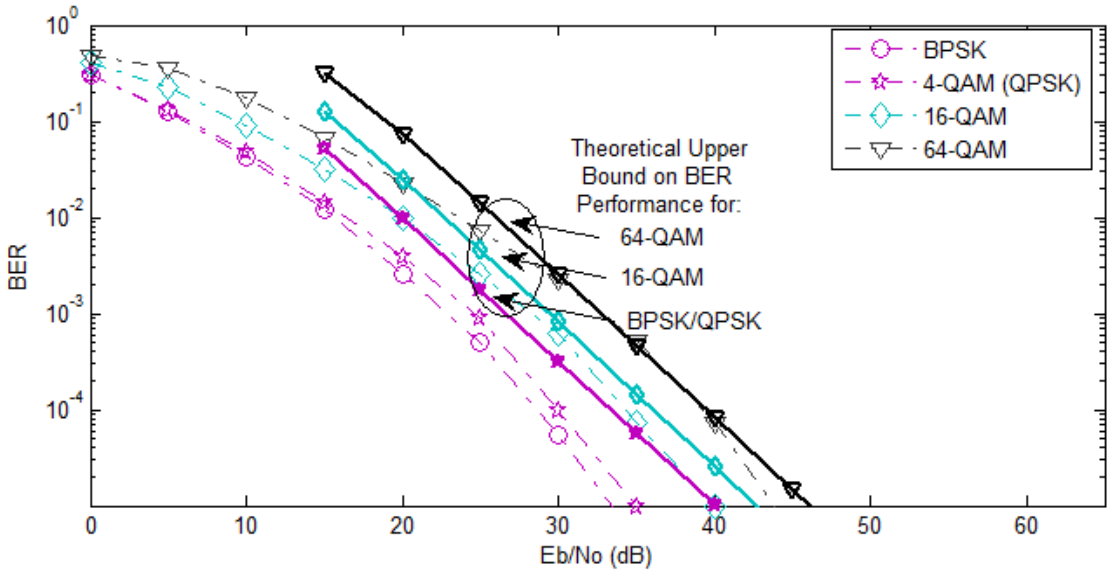

Figure 3.6: BER performance of convolutionally encoded BPSK, 4-QAM, 16-QAM and 64-QAM under flat Rayleigh fading conditions with $\mathcal{R}_C = 2/3$.

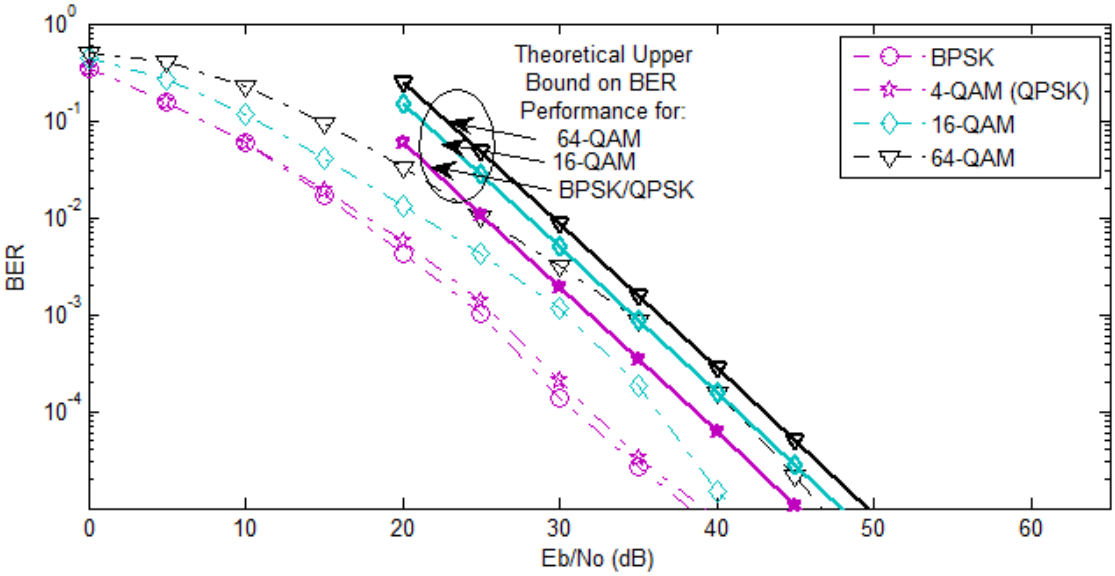

Figure 3.7: BER performance of convolutionally encoded BPSK, 4-QAM, 16-QAM and 64-QAM under flat Rayleigh fading conditions with $\mathcal{R}_C = 3/4$.

3.1.4 Assumptions

In this study, we are interested in measuring the average PSNR due to quantization and transmission errors. Therefore in what follows we assume error-free headers and markers. This is can be done using powerful error correcting codes. In addition, we assume that the feedback channel is highly reliable, as a result control messages and channel information arrive at the transmitter free of errors. This is also justified by assuming that a sufficiently powerful error-control code is employed to ensure error free transmission on the backward channel.

3.2 Proposed Transmission Scheme

When a fixed-modulation technique is used independent of the channel state, a conservative design would consider the worst case scenario and use a modulation level that gives an acceptable immunity for all channel conditions. As the condition of the channel improves, using a fixed-modulation mode will render the system to be spectrally inefficient. This is explained by the fact that using a low modulation level during the "good" channel conditions will hinder the transmission at higher data rates that would have been possible if the proper modulation mode have been used. Thus, in the proposed transmission scheme adaptive modulation is adopted to maximize the spectral efficiency while maintaining a predefined target BER as the channel conditions vary with time.

In addition to adaptive modulation, channel coding is adaptively employed to provide an extra protection and extend the performance to the poor channel SNR range that even very low modulation levels cannot serve effectively. In this work, we consider convolutional coding as the channel coding technique. The code rate is changed from one packet to another according to the channel conditions and the importance of the transmitted bit stream. More specifically, high modulation levels and high coding rates are used when the channel conditions are favorable and lower modulation levels and lower coding rates as the channel condition worsens.

To determine the most appropriate modulation mode and coding rate, the proposed scheme partitions the received SNR space by setting different thresholds on the SNR values. In what follows the term SNR refers to the ratio of average energy per bit to noise power spectral density (E_b/N_0). Based on the received SNR ($\dot{\gamma}$) and the priority of the bitstream, the appropriate modulation mode and code rate will be selected for next transmission. Let the priority of a bit stream i be $\mathcal{P}_i$ where $i \in [1, 2, 3, ..., q]$ and $\mathcal{P}_1 > \mathcal{P}_2 > \mathcal{P}_3... > \mathcal{P}_q$. Denote the modulation level by $\mathcal{L}_M$ and also denote the channel coding rate by $\mathcal{R}_C$. The most important bitstream is assigned the highest priority $\mathcal{P}_1$ with the lowest target BER, the second most

important bitstream is assigned the priority $\mathcal{P}_2$ with the second lowest BER, while the least important bitstream is assigned the priority $\mathcal{P}_q$ with the highest target BER. Thus, for a certain SNR value, a lower modulation level and powerful coding rate (i.e. low BER) will be typically used for the bitstream with $\mathcal{P}_1$ while higher modulation levels and higher coding rates will be used for the other bitstreams with priorities $\mathcal{P}_2, \mathcal{P}_3, ..., \mathcal{P}_q$, respectively. The pseudo-code for the proposed adaptive algorithm is given below:

1. Divide the source encoder output into q-bitstreams with unequal importance
   for i=1, ..., q
   2. Determine the priority of the bitstream $\mathcal{P}_i$
   3. Determine the desired target BER for each bitstream
   4. Find the SNR Thresholds to achieve the target BERs
   5. Get the estimate of the channel SNR ($\grave{\gamma}$)
   6. Compare ($\grave{\gamma}$) against the SNR thresholds
   7. Select the appropriate $\mathcal{L}_M$ and $\mathcal{R}_C$
   end for
8. **return**

Figure 3.8: Algorithm to adapt the parameters of the purposed model.

We assume that the channel is a Rayleigh flat-fading channel that does not change during the packet transmission period. Thus, the equivalent received signal can be expressed as:

$$r(t) = \sum_{i=1}^{q} \sum_{k=1}^{K_i} g_{ki}(t) + n(t), \tag{3.22}$$

where q is the number of the bitstreams, K_i is the number of data blocks within a bitstream, $n(t)$ denotes the complex AWGN noise with zero mean and $N_0/2$ variance and $g_{ki}(t)$ denotes the k^{th} transmitted signal with priority $\mathcal{P}_i$ which can be expressed as:

$$g_{ki}(t) = \sum_{j=1}^{J_k} \alpha_{jk}^{(i)} c_{jk}^{(i)}, \tag{3.23}$$

where J_k is number of symbols within the k^{th} block of data, $\alpha_{jk}^{(i)}$ represents the fading coefficients of the Rayleigh channel, and $c_{jk}^{(i)}$ denotes the j^{th} symbol. At the receiver,

the signal is demodulated, decoded and combined to reconstruct the received data.

In order to appropriately select the transmission parameters for the next transmission, CSI at the receiver is fed back to the transmitter via a reliable and error-free feedback channel. The transmitter then decides on the modulation level and the coding rate based on the fed back CSI and the priority of the bitstream along with the target BER.

3.2.1 Image Transmission Using Adaptive Modulation Scheme

In this section, we develop an image transmission scheme using adaptive modulation only according to the proposed methodology. The compressed bitstream of the encoded image is divided into three priority-levels bitstreams (i.e. with unequal importance). The priority of a bit stream i is $\mathcal{P}_i$ where $i \in [1, 2, 3]$ and $\mathcal{P}_1 > \mathcal{P}_2 > \mathcal{P}_3$. The first bitstream contains the DC coefficients, which represents the average luminance of the 8×8 blocks of the image. These DC coefficients are the most important information. The second bitstream contains the low-frequency AC coefficients which are concentrated in the upper left parts of each of the 8×8 blocks of the image. With the low-frequency AC coefficients most of the details of the image could be recovered, however, they are less important than the DC coefficients. The third bitstream carries the high-frequency AC coefficients which generally represent the fine details of the image. Since the human visual system is less sensitive to high frequency components (i.e. fine details), they are considered to be the least significant data.

Since the bitstream for the DC coefficients is the most important stream, it is assigned the priority $\mathcal{P}_1$ with target BER of 10^{-5}, the second bitstream with the low-frequency coefficients is assigned the priority $\mathcal{P}_2$ with target BER of 10^{-4} while the third bitstream with the high-frequency coefficients is assigned the priority $\mathcal{P}_3$ with target BER of 10^{-3}. Thus, for a certain SNR value, a lower modulation level (i.e. lower BER) is typically used for the bitstream with $\mathcal{P}_1$ while higher modulation levels are used for the other two bitstreams that contain the low and high frequency AC coefficients with priorities $\mathcal{P}_2$ and $\mathcal{P}_3$, respectively.

In this algorithm, the modulation level is selected from one of the following levels: $\mathcal{L}_M \in [2, 4, 16, 64]$. As illustrated in Figure 3.9 the thresholds on the estimated SNR ($\grave{\gamma}$) were derived from the theoretical BER performance of various modulation levels over Rayleigh fading channel. For instance, if the desired BER is 10^{-3} and $\grave{\gamma}$

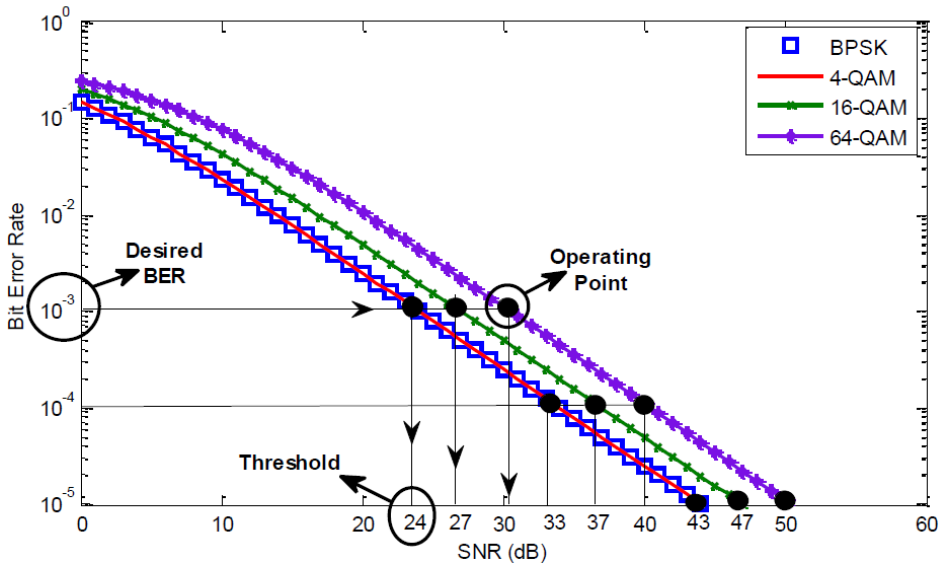

Figure 3.9: Theoretical BER performance of BPSK, 4-QAM, 16-QAM and 64-QAM under flat Rayleigh fading conditions.

at the receiver falls below 24 dB then BPSK is to be used. While in cases $\grave{\gamma}$ falls between 24 dB and 27 dB the system uses 4-QAM. As the channel condition gets better, 16-QAM could be used when $\grave{\gamma}$ falls between 27 dB and 30.5 dB, while 64-QAM is selected beyond 30.5 dB. Therefore, each time a block of data is ready for transmission, the transmitter gets the estimate of SNR from the receiver, checks the priority of the bitstream to decide the desired BER and decides the needed modulation level. The decision involves a lookup table to speedup the selection process of the proper modulation level. Table 3.5 shows the proper modulation levels for different thresholds of the estimated SNR which satisfies the requirement of maintaining a target BER. The SNR thresholds are selected based on the theoretical performance of various modulation levels over Rayleigh fading channel as illustrated in Figure 3.9. The results of this analysis will be presented in Chapter 4.

Table 3.5: Look-up table to achieve BERs of 10^{-5}, 10^{-4} and 10^{-3} using adaptive modulation.

Threshold on received SNR to achieve BER of 10^{-5}	Modulation level
$\grave{\gamma} \leqslant 43.0$ dB	BPSK
$43.0\ dB < \grave{\gamma} \leqslant 47.0\ dB$	4-QAM
$47.0\ dB < \grave{\gamma} \leqslant 50.0\ dB$	16-QAM
$50.0\ dB < \grave{\gamma}$	64-QAM
Threshold on received SNR to achieve BER of 10^{-4}	**Modulation level**
$\grave{\gamma} \leqslant 33.0$ dB	BPSK
$33.0\ dB < \grave{\gamma} \leqslant 37.0\ dB$	4-QAM
$37.0\ dB < \grave{\gamma} \leqslant 40.0\ dB$	16-QAM
$40.0\ dB < \grave{\gamma}$	64-QAM
Threshold on received SNR to achieve BER of 10^{-3}	**Modulation level**
$\grave{\gamma} \leqslant 24.0$ dB	BPSK
$24.0\ dB < \grave{\gamma} \leqslant 27.0\ dB$	4-QAM
$27.0\ dB < \grave{\gamma} \leqslant 30.5\ dB$	16-QAM
$30.5\ dB < \grave{\gamma}$	64-QAM

3.2.2 Multimedia Transmission Using Joint Adaptive Modulation and Channel Coding Scheme

The proposed adaptive modulation scheme in the previous section was extended by employing adaptive convolutional channel coding where the code rates are chosen based on the channel conditions as well as the importance of the bitstream. In this scheme, the modulation level and the channel coding rate are $\mathcal{L}_M \in [2, 4, 16, 64]$ and $\mathcal{R}_C \in [1/3, 1/2, 2/3, 3/4]$, respectively. Lookup table was generated and used for the selection process of the optimal transmission parameters that achieve the desired BER while maximizing the bandwidth efficiency. This table was developed by simulating BER performance curves of the used modulation schemes and channel coding rates

in Rayleigh flat-fading channel to achieve a set of BERs. Then for each predefined BER, we determined the corresponding SNR thresholds as shown in Figures 3.10, 3.11 and 3.12 for a target bit error rate as 10^{-3}, 10^{-4} and 10^{-5}, respectively.

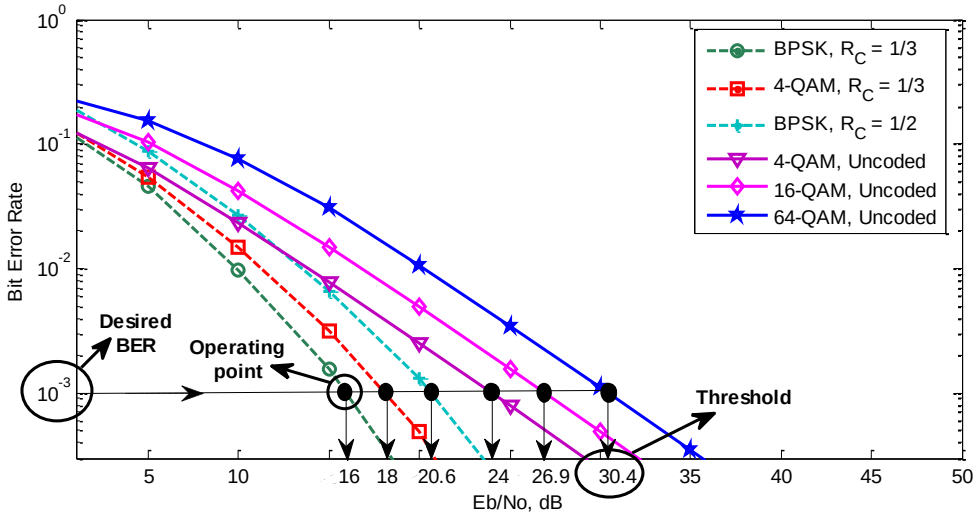

Figure 3.10: BER performance for various coded modulation schemes under flat Rayleigh fading conditions.

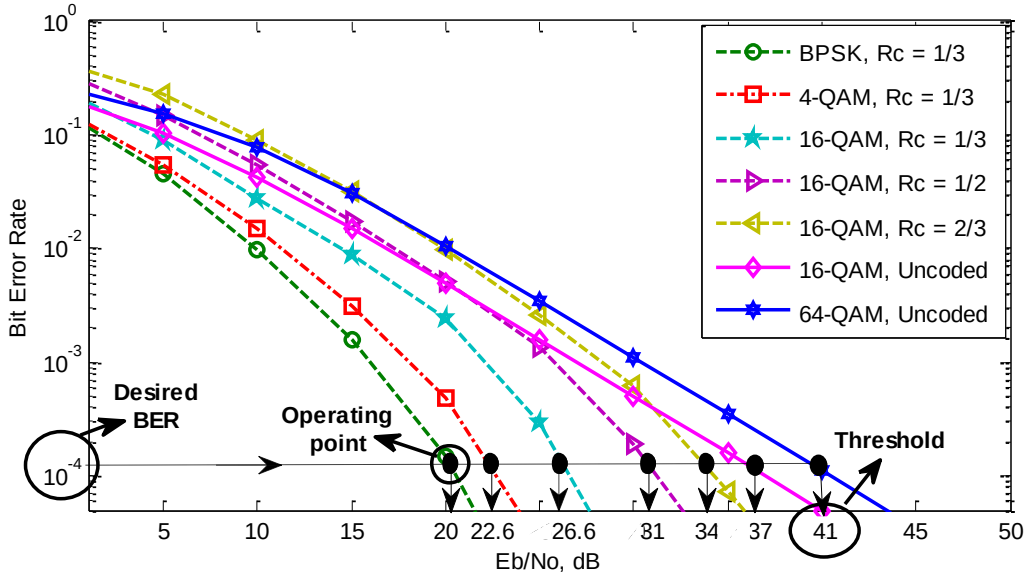

Figure 3.11: BER performance for various coded modulation schemes under flat Rayleigh fading conditions.

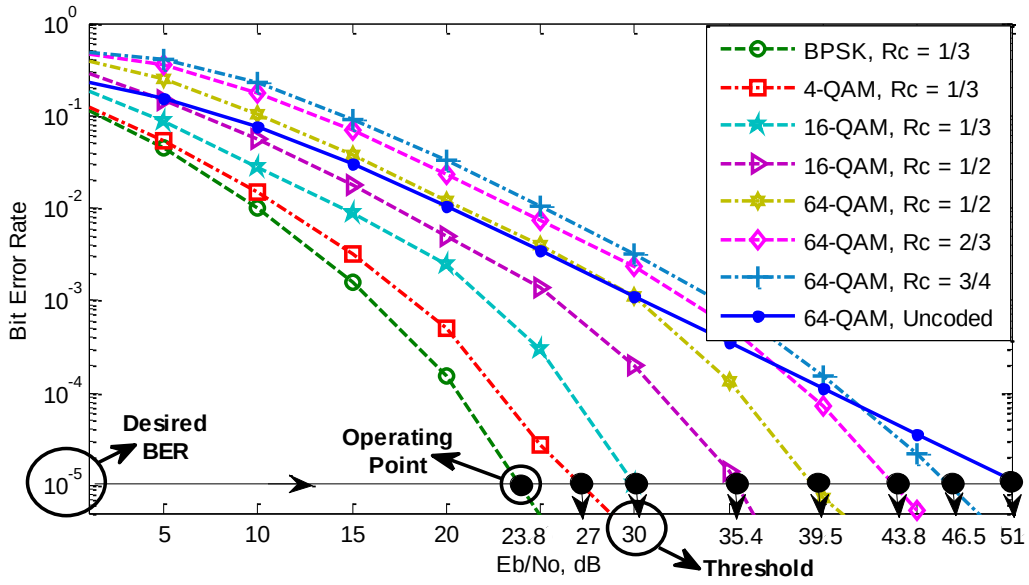

Figure 3.12: BER performance for various coded modulation schemes under flat Rayleigh fading conditions.

For instance, if the desired BER is 10^{-5} and the estimated SNR ($\grave{\gamma}$) at the receiver falls between 27 dB and 30 dB the system uses 4-QAM with $\mathcal{R}_C = 1/3$. While in the case when $\grave{\gamma}$ falls between 30 dB and 35.4 dB the system will use 16-QAM with $\mathcal{R}_C = 1/3$. However, as the channel condition gets better, higher data rates and higher channel code rates could be used such as 64-QAM with $\mathcal{R}_C = 2/3$ when $\grave{\gamma}$ falls between 43.8 dB and 46.5 dB, or 64-QAM with $\mathcal{R}_C = 3/4$ when $\grave{\gamma}$ falls between 46.5 dB and 51.0 dB. Clearly, beyond 51.0 dB uncoded 64-QAM is sufficient to achieve the target BER. It should be mentioned here that as long as $\grave{\gamma}$ is below 23.8 dB, and hence the channel does not allow us to guarantee the predefined target BER, always BPSK with $\mathcal{R}_C = 1/3$ will always be used to achieve the best possible BER performance. According to the empirically derived values reported in Table 3.6, $\grave{\gamma}$ is compared against the SNR thresholds to choose the optimal transmission parameters that provide the highest bandwidth efficiency (i.e. highest modulation level with highest coding rate possible) for the predefined target BER. Therefore, each time a block of data is ready for transmission, the transmitter checks the priority of the bitstream to decide the desired BER, gets the estimate of the channel SNR from the

receiver to compare it against the SNR thresholds in the lookup tables, and selects the transmission parameters to be employed.

Table 3.6: Look-up table to achieve BERs of 10^{-3}, 10^{-4} and 10^{-5} using the adaptive modulation and channel coding scheme.

Threshold on received SNR to achieve BER of 10^{-5}	Modulation mode	Code rate
$\grave{\gamma} < 27.0\ dB$	BPSK	1/3
$27.0\ dB < \grave{\gamma} < 30.0\ dB$	4-QAM	1/3
$30.0\ dB < \grave{\gamma} < 35.4\ dB$	16-QAM	1/3
$35.4\ dB < \grave{\gamma} < 39.5\ dB$	16-QAM	1/2
$39.5\ dB < \grave{\gamma} < 43.8\ dB$	64-QAM	1/2
$43.8\ dB < \grave{\gamma} < 46.5\ dB$	64-QAM	2/3
$46.5\ dB < \grave{\gamma} < 51.0\ dB$	64-QAM	3/4
$51.0\ dB < \grave{\gamma}$	64-QAM	Uncoded
Threshold on received SNR to achieve BER of 10^{-4}	Modulation mode	Code rate
$\grave{\gamma} < 22.6$ dB	BPSK	1/3
$22.6\ dB < \grave{\gamma} < 26.6\ dB$	4-QAM	1/3
$26.6\ dB < \grave{\gamma} < 31.0\ dB$	16-QAM	1/3
$31.0\ dB < \grave{\gamma} < 34.0\ dB$	16-QAM	1/2
$34.0\ dB < \grave{\gamma} < 37.0\ dB$	16-QAM	2/3
$37.0\ dB < \grave{\gamma} < 41.0\ dB$	16-QAM	Uncoded
$41.0\ dB < \grave{\gamma}$	64-QAM	Uncoded
Threshold on received SNR to achieve BER of 10^{-3}	Modulation mode	Code rate
$\grave{\gamma} < 18.0\ dB$	BPSK	1/3
$18.0\ dB < \grave{\gamma} < 20.6\ dB$	4-QAM	1/3
$20.6\ dB < \grave{\gamma} < 24.0\ dB$	BPSK	1/2
$24.0\ dB < \grave{\gamma} < 26.9\ dB$	4-QAM	Uncoded
$26.9\ dB < \grave{\gamma} < 30.4\ dB$	16-QAM	Uncoded
$30.4\ dB < \grave{\gamma}$	64-QAM	Uncoded

3.2.2.1 Image Transmission Using Joint Adaptive Modulation and Channel Coding Scheme

Lena, Clown and Cathrine images are used to asses the quality of the transmitted images using the proposed scheme. It was found out that it is only sufficient to divide the image compressed bitstreams into two priority levels. The first bitstream contains the DC coefficients and assigned the priority $\mathcal{P}_1$ with a target BER of 10^{-5}. The second bitstream contains the low-frequency AC coefficients and assigned the priority $\mathcal{P}_2$ with a target BER of 10^{-4}. In this analysis, we trimmed the high-frequency AC coefficients considering the fact that the human visual system is less sensitive to the information contained in these coefficients. This can be shown in Table 3.7 which compares PSNR of different reconstructed compressed images to the $PSNR_T$ (dB) of the reconstructed images using the DC and the low frequency coefficients (i.e. with trimmed high-AC coefficients). Obviously, in terms of PSNR the impact of the high-frequency AC coefficients is insignificant on the quality of the reconstructed images. The results of this analysis will be presented in Chapter 4.

Table 3.7: Comparison of PSNR results for JPEG algorithm

Image	PSNR (dB)	PSNR$_T$ (dB)
Lena	32.897	32.244
Clown	36.769	36.655
Cathrine	31.053	30.276

3.2.2.2 Video Transmission Using Joint Adaptive Modulation and Channel Coding Scheme

The H.264 standard includes a data partitioning technique that divides the compressed data into separate units of different importance. Generally, all MBs are coded together in a single bit string that forms a slice. However, data partitioning mode allows the partitioning of a normal slice in up to three partitions, so that each

part can be paired accordingly with UEP during transmission. These partitions are defined as follow:

- Partition (A): contains the slice header, motion vectors, prediction modes, quantization parameters, and MB types. The corruption of partition (A) leads to the loss of the entire video slice, including partitions (B) and (C). Hence, this information is considered to be the most important.

- Partition (B): contains the intra-coded MB coefficients. Intra-coded partitions can stop further error propagation however they are less important than the information of type (A) partition. Their use requires the presence of partition (A) in order to be decoded.

- Partition (C): contains the inter-coded MB coefficients which considered to be the least important information since it does not resynchronize the encoder and the decoder. The availability of partition (A) is required to decode partition (C).

As a result, partition (A) data has to be protected with the highest priority while partitions (B) and (C) data are of lower priority. Thus, the compressed bitstream of the encoded video is divided into three priority-levels bitstreams. The first bitstream contains the information of partition (A) and assigned the priority $\mathcal{P}_1$ with a target BER of 10^{-5}. The second bitstream contains the information of partition (B) and assigned the priority $\mathcal{P}_2$ with a target BER of 10^{-4}. The third bitstream contains the information of partition (C) and assigned the priority $\mathcal{P}_3$ with a target BER of 10^{-3}. The results for video transmission will be presented in Chapter 4.

Chapter 4

Performance Analysis

4.1 Image Transmission Using Adaptive Modulation

To evaluate the performance of the proposed adaptive modulation scheme, we simulated the transmission of the 256×256 JPEG-compressed gray scale Lena image. The compressed bitstream of the encoded image is divided into three priority-levels bitstreams as described earlier in Chapter 3. Each bitstream is modulated according to the proposed scheme and transmitted over a Rayleigh flat-fading channel. At the receiver, the signal is demodulated, decoded and combined to reconstruct the received image.

4.1.1 Simulation Results

Figure 4.1 compares the average BER of the proposed adaptive modulation scheme with the BER of the conventional BPSK modulation scheme versus the channel SNR. The figure indicates that the performance of the proposed scheme is comparable to the performance of BPSK at low SNR values while the BER increases at higher SNR values. This behavior is simply explained by the fact that at low SNR values, the proposed scheme tends to use lower modulation levels (typically BPSK) and thus results in BER that is close to that of BPSK. At higher SNR values, the proposed scheme employs higher modulation levels which in turn yield improved spectral efficiency at the expense of reasonably increased BER.

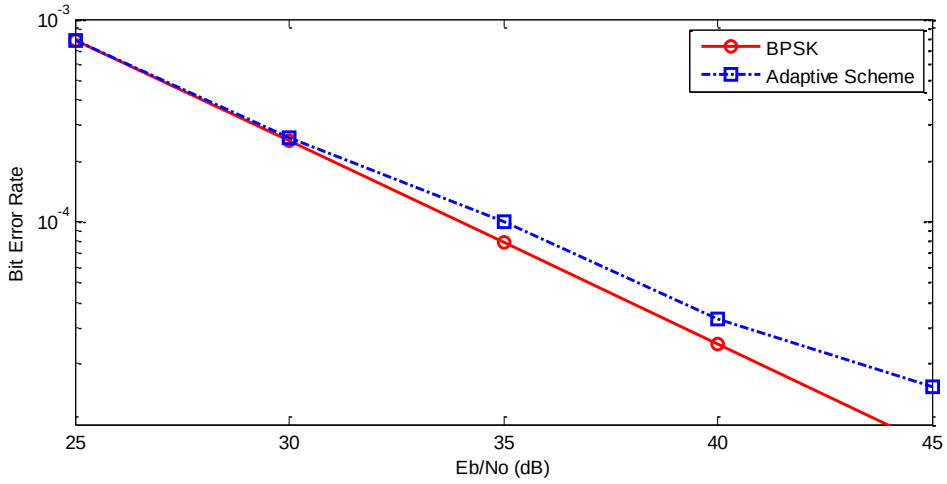

Figure 4.1: The average BER performance of the adaptive modulation scheme under flat Rayleigh fading conditions.

Figure 4.2 compares the achievable spectral efficiency of the proposed scheme over Rayleigh fading channel with the spectral efficiencies of BPSK, 4-QAM, 16-QAM and 64-QAM fixed modulation schemes. Clearly, as the SNR increases, there is an increasing trend in the Bandwidth efficiency of the proposed adaptive modulation scheme over the fixed-modulation based systems.

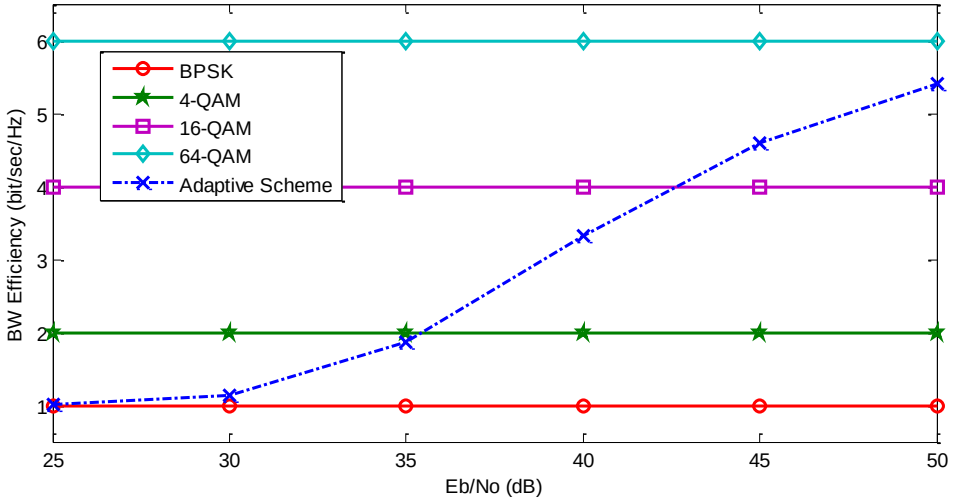

Figure 4.2: The average spectral efficiency of the adaptive modulation scheme under flat Rayleigh fading conditions.

Figure 4.3 demonstrates the impact on the subjective (visual) quality of transmitted image using adaptive modulation. In addition, and for the sake of comparison, the BPSK fixed modulation scheme with different SNR values was used for the transmission of the same image.

(a) PSNR = 23.32068dB (b) PSNR = 29.05831 dB (c) PSNR = 32.8969 dB

(d) PSNR = 19.9738 dB
r = 1.8411 bit/sec/Hz

(e) PSNR = 26.2580 dB
r = 3.2749 bit/sec/Hz

(f) PSNR = 30.2931dB
r = 4.5906 bit/sec/Hz

Figure 4.3: Transmitted Lena image over Rayleigh fading channel using adaptive scheme.

Figures 4.3-(a), 4.3-(b), and 4.3-(c) show the reconstructed images using fixed BPSK modulation scheme with constant bandwidth efficiency $r = 1.0$ Bits/sec/Hz and average SNR values 35 dB, 40 dB, and 45 dB, respectively. Intuitively, the PSNR of the reconstructed images increases with the increase in the SNR values. Figures 4.3-(d), 4.3-(e), and 4.3-(f) show the reconstructed images using the proposed adaptive modulation scheme for average SNR values 35 dB, 40 dB, and 45 dB, respectively. Clearly, the spectral efficiency increases as the SNR increases. While Figures 4.3-(d) to 4.3-(f), show less PSNR values when compared to Figures 4.3-(a) to 4.3-(c), their associated spectral efficiency is always higher. This is actually a desirable trend

especially when the proposed scheme is extended for video transmission over fading channels.

Figures 4.4 compares the PSNR for the proposed adaptive scheme with that of the BPSK fixed modulation scheme. PSNR is an objective quality measure used to judge the quality of the reconstructed image. It measures the difference between the original and the reconstructed image. The PSNR in dB is given by:

$$PSNR = 10\log_{10}\left(\frac{255^2}{\frac{1}{XY}\sum_{x=0}^{X-1}\sum_{y=0}^{Y-1}[\grave{I}(x,y) - I(x,y)]^2}\right), \tag{4.1}$$

where X and Y are the number of rows and columns respectively, in the input images $\grave{I}$ and I.

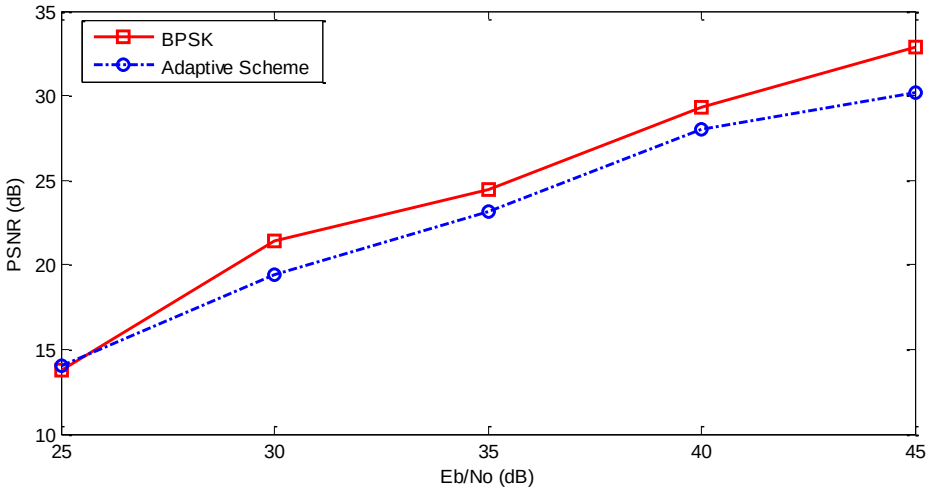

Figure 4.4: The average PSNR performance of the adaptive modulation scheme under flat Rayleigh fading conditions.

Figure 4.4 also shows that the proposed adaptive scheme achieves PSNR values that are less than those of the fixed BPSK system by no more than 3 dB. While this drop in the achieved PSNR is not of a major impact on the achieved perceptual quality, it must be noted that the achieved data rates is much higher than the case of BPSK. This is desirable when high data rate video information is transmitted. The quality degradation in the reconstructed image can be seen by comparing Figure 4.3-(c) and

Figure 4.3-(f). While the PSNR of the image in Figure 4.3-(f) is 2.6 dB less than that in Figure 4.3-(c), it is still of good and acceptable quality. At the same time, the achieved spectral efficiency associated with the image in Figure 4.3-(f) is about 460% of that in Figure 4.3-(c), which is another advantage of the proposed adaptive scheme over fixed modulation schemes.

4.2 Image Transmission Using Joint Adaptive Modulation and Channel Coding

Image transmission using joint adaptive modulation and channel coding was also evaluated through simulating the transmission of 256×256 JPEG-compressed gray scale Lena, Clown and Cathrine images over a Rayleigh flat-fading channel.

4.2.1 Simulation Results

Figure 4.5 illustrates the average BER performance of the adaptive modulation and channel coding scheme versus the average channel SNR for three different BER constraints.

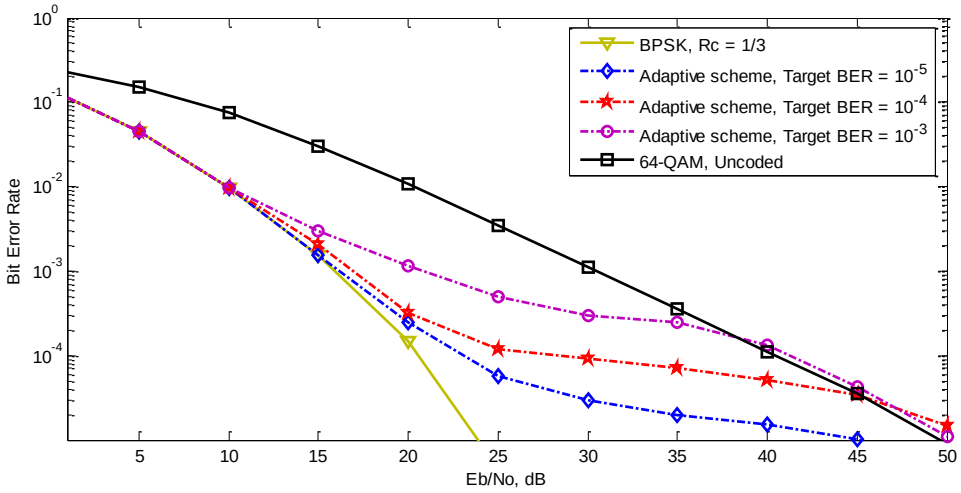

Figure 4.5: The average BER performance of the adaptive modulation and channel coding scheme under flat Rayleigh fading conditions.

Clearly, BPSK with $\mathcal{R}_C = 1/3$ is the most robust combination in terms of BER performance. However, it reduces the bandwidth efficiency of the system to $r = 1/3$ Bit/sec/Hz, which is relatively low for video applications. In contrast, while 64-QAM is spectrally more efficient it requires relatively high channel SNR values for a better BER performance. It can be seen also that the adaptive approach closely follows the corresponding target BER while attempting to optimize the spectral efficiency. Figure 4.6 compares the achievable spectral efficiency of the adaptive scheme for desired BERs of 10^{-3}, 10^{-4} and 10^{-5} with the spectral efficiencies of BPSK with $\mathcal{R}_C = 1/3$ and 64-QAM fixed modulation schemes. It can be seen that as the SNR increases,

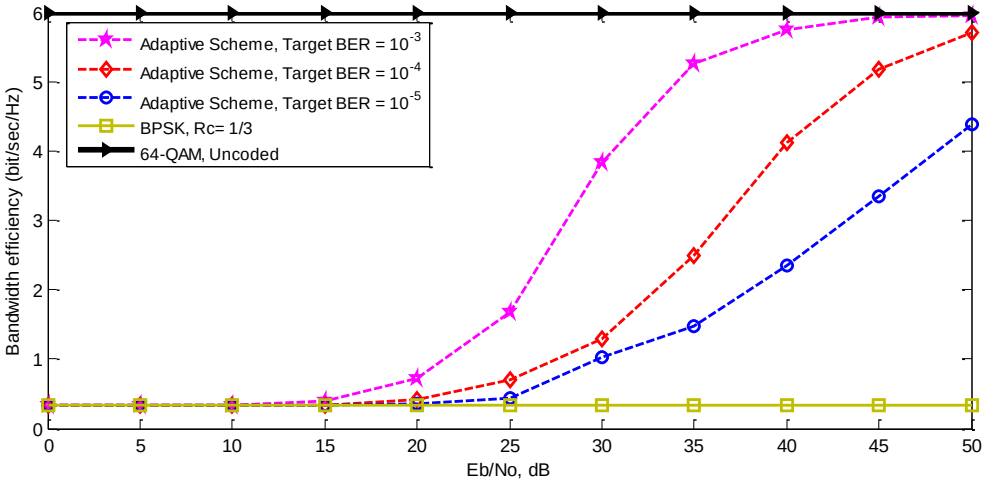

Figure 4.6: The average spectral efficiency of the adaptive modulation and channel coding scheme under flat Rayleigh fading conditions.

there is an increasing trend in the bandwidth efficiency of the proposed adaptive scheme. Besides, lowering the target BER allows a higher effective spectral efficiency. This is desirable especially for wireless video applications, since they are delay and loss sensitive applications, and such an adaptive approach is expected to reasonably maintain the tradeoff between the data rate and loss rate.

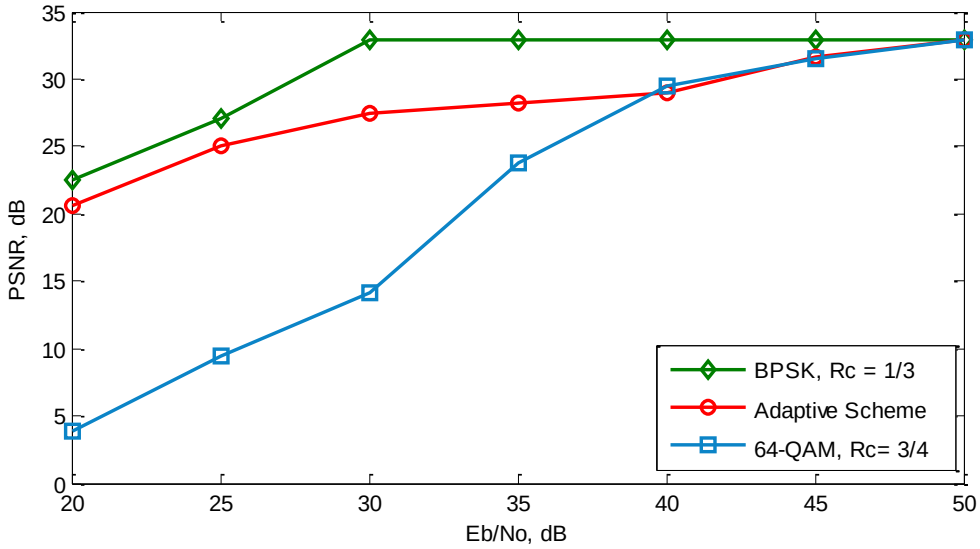

Figure 4.7: The average PSNR performances for Lena image using adaptive modulation and channel coding scheme under flat Rayleigh fading conditions.

Figures 4.7 and 4.8 demonstrate the impact of the adaptive modulation and channel coding scheme on the objective and subjective (visual) quality of transmitted images. Figure 4.7 shows the average PSNR for a JPEG-compressed Lena image as a function of channel SNR. This figure shows that BPSK with $\mathcal{R}_C = 1/3$ constitutes an upper bound on the achieved PSNR and hence it will be considered as the target to be achieved. Following the same argument, 64-QAM with $\mathcal{R}_C = 3/4$ will constitute a lower bound on the achievable PSNR. The figure also shows that for low SNR values, the achieved PSNR of the proposed adaptive scheme ranges 1.5 to 4.5 dB below the upper bound of BPSK with $\mathcal{R}_C = 1/3$. While for high SNR values the proposed scheme is identical to the high rate 64-QAM with $\mathcal{R}_C = 3/4$.

Figures 4.8 shows three reconstructed images using the adaptive scheme associated with their spectral efficiencies. Images in Figures 4.8-(a), 4.8-(d), and 4.8-(g) were transmitted at an average SNR value of 35 dB, images in Figures 4.8-(b), 4.8-(e), and 4.8-(h) were transmitted at an average SNR value of 40 dB while images in Figures 4.8-(c), 4.8-(f), and 4.8-(i) were transmitted at an average SNR value of 45 dB. As can be seen from the figures, the visual quality, the PSNR and the spectral

efficiency improve as the SNR increases.

(a) PSNR = 21.39 dB
r = 0.38 bit/sec/Hz

(b) PSNR = 26.64 dB
r = 1.30 bit/sec/Hz

(c) PSNR = 32.10 dB
r = 3.91 bit/sec/Hz

(d) PSNR = 26.16 dB
r = 0.40 bit/sec/Hz

(e) PSNR = 30.55 dB
r = 1.24 bit/sec/Hz

(f) PSNR = 32.74 dB
r = 3.90 bit/sec/Hz

(g) PSNR = 21.88 dB
r = 0.43 bit/sec/Hz

(h) PSNR = 28.81 dB
r = 1.26 bit/sec/Hz

(i) PSNR = 30.05 dB
r = 3.96 bit/sec/Hz

Figure 4.8: Transmitted images over Rayleigh fading channel using adaptive modulation and channel coding scheme.

The average PSNRs versus the average channel SNR for the three images are shown in Figure 4.9. The PSNR values of the decoded Lena, Clown and Cathrine images without transmission are 32.2 dB, 36.6 dB and 30.2 dB, respectively. These

PSNRs are the upper bound of the simulation results. We can notice that the achieved PSNR values for Catherine image are better than those for Lena image at low channel SNRs, while the situation is reversed at high channel SNRs. This behavior could be explained by fact that we maintained the same number of coefficients for the three images which could not be enough because of the different inherited details in each image. Obviously, the three curves in Figure 4.9 show the same trend, which demonstrate that the application of the proposed scheme is independent of the transmitted image.

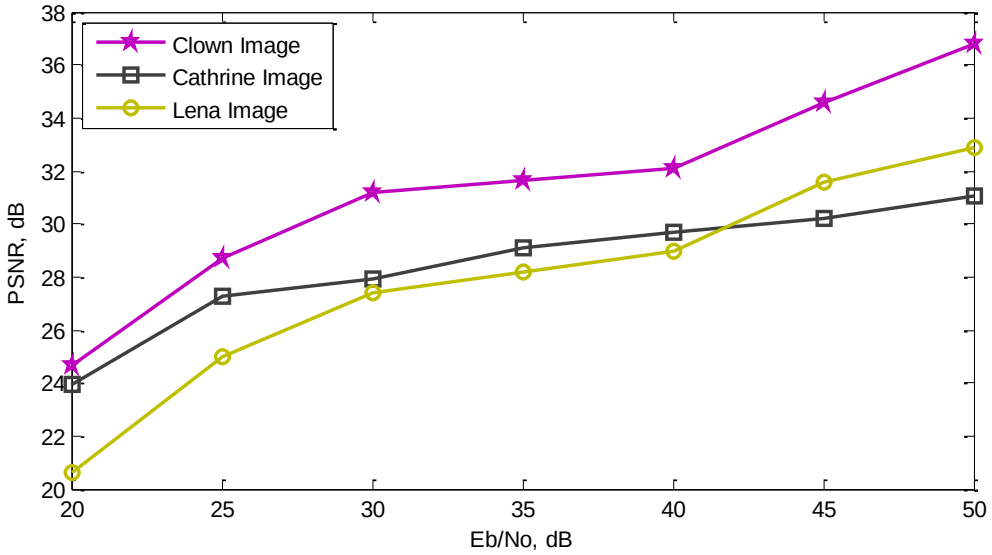

Figure 4.9: The average PSNR performances using adaptive modulation and channel coding scheme under flat Rayleigh fading conditions.

4.3 Video Transmission Using Joint Adaptive Modulation and Channel Coding

The performance of the joint adaptive modulation and channel coding scheme was evaluated for video transmission. This was done through simulating the transmission of 352×288 pixel common intermediate format (CIF) for different video sequences.

4.3.1 Simulation Results

Figures 4.10 and 4.11 show the subjective and objective quality for three different video sequences. Figure 4.10 presents snapshots of the received Bus, Soccer and Bridge videos. Figures 4.10-(a), 4.10-(c), and 4.10-(e) are the locally decoded frames, while Figures 4.10-(b), 4.10-(d), and 4.10-(f) are the received video frames.

(a) (b) (c) (d) (e) (f)

Figure 4.10: Snapshot of three video sequences using adaptive modulation and channel coding scheme under flat Rayleigh fading conditions.

It can be seen that the proposed adaptive transmission scheme maintains an acceptable visual quality for the three video sequences.

Figure 4.11 depicts the PSNR for 150 frames of the "Bus" sequence coded at 25 frames/sec when transmitted using the proposed scheme under flat Rayleigh fading conditions. The video sequence was transmitted at 25 dB, 35 dB and 45 dB

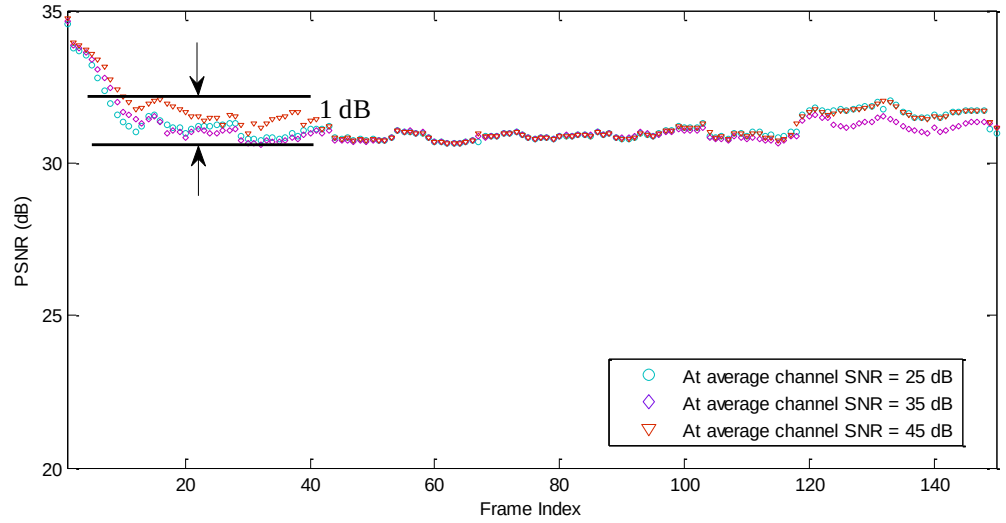

Figure 4.11: The average PSNR performances of "Bus" video sequence using adaptive modulation and channel coding scheme under flat Rayleigh fading conditions.

average channel SNRs. The result indicates that the PSNR curves are close in the three cases and achieve relatively high values. The PSNR values change smoothly and less frequently which consequently gives a better presentation to the viewer. Hence, an advantage of the proposed scheme is that the playback quality of the decoded frames is smooth. Although the simulation were carried for a wide SNR range (25 to 45 dB), it can be seen that the resultant PSNR swings in a range less than 1-dB which demonstrates the reliability and the robustness of our model.

Figure 4.12 depicts the spectral efficiency achieved by the proposed adaptive algorithm as a function of the average channel SNR. It also shows the spectral efficiency of BPSK with $\mathcal{R}_C = 1/3$ which constitutes a lower bound on the achieved spectral efficiency. Following the same argument, 64-QAM modulation scheme will

constitute an upper bound on the achievable bandwidth efficiency and hence it will be considered as the target to be achieved. It can be seen that high levels of SNR

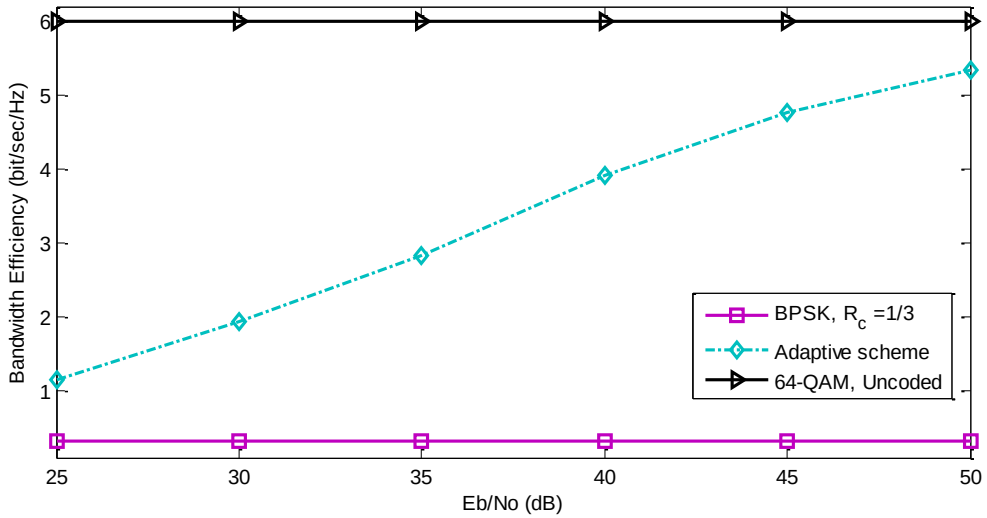

Figure 4.12: The average spectral efficiency of "Bus" sequence using adaptive modulation and channel coding scheme under flat Rayleigh fading conditions.

increases the bandwidth efficiency which allows higher transmission rates. This is explained by the fact that as the channel condition enhances, the proposed scheme tends to use higher modulation modes (i.e. higher data rates) with higher coding rates to maximize the achievable transmission rate. As expected, the spectral efficiency is not governed by the minimum data rate constraint which is $\frac{1}{3}$ bit/sec/Hz and is not exceeding the maximum possible data rate which is 6 bit/sec/Hz. It has been our goal to achieve performance close to the upper limit in terms of bandwidth efficiency while having a minimal impact on the video quality as illustrated in Figures 4.10, 4.11 and 4.12.

4.4 Sensitivity Evaluation

Channel state information (CSI) is obviously very critical in our approach. The channel must be estimated at the receiver and then the CSI is fed back to the transmitter via a feedback channel. Throughout this research, it is assumed that the receiver has

perfect knowledge of the channel which may not be valid. In practice, the channel estimation is often imperfect due to noise, interference and the time-varying nature of the wireless channel. Therefore, it is important to investigate the robustness of the proposed scheme to channel estimation errors.

In this simulation, estimation errors are introduced by adding ±3 dB and ±5 dB constantly to the estimated channel SNR at the receiver before it is sent via the feedback channel. At the transmitter, the available CSI is used to adapt the modulation modes and the code rates as explained earlier.

Figure 4.13 shows the effects of channel estimation errors on the average bit error probability of the proposed scheme and compare it with the performance in the presence of a perfect CSI. It can be observed that the proposed model with ±3 dB estimation errors, has a performance that is close to the one with ideal channel information at a BER of 10^{-4}.

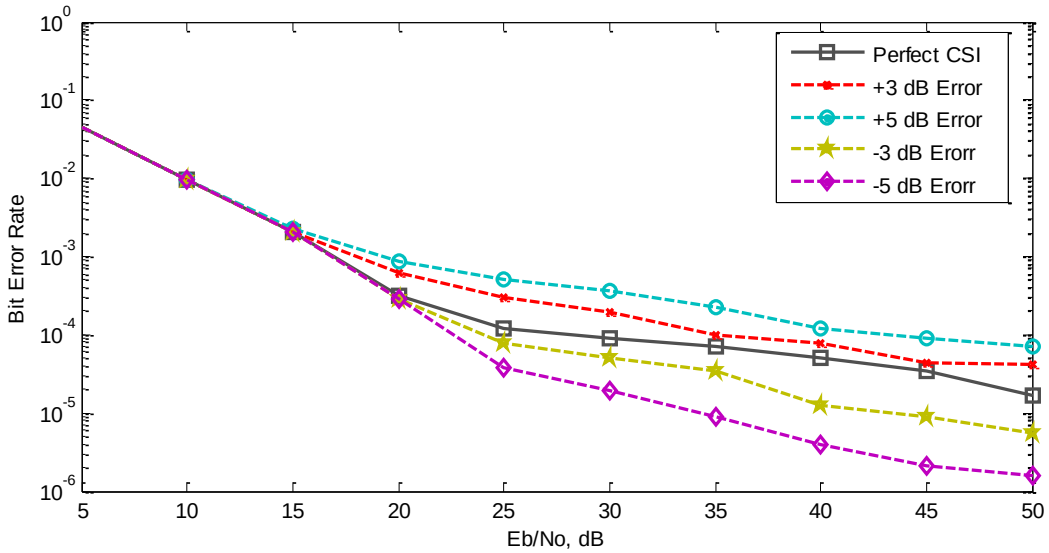

Figure 4.13: The average BER performance of the adaptive modulation and channel coding scheme for target BER of 10^{-4} over Rayleigh fading channel.

Figure 4.14 shows the effects of channel estimation errors on the average spectral efficiency of the proposed scheme for target BER of 10^{-4} and compare it with the performance in the presence of a perfect CSI. We can notice that if the channel SNR

is underestimated, this would result in graceful reduction in the bandwidth efficiency. While overestimating the channel SNR would result in higher bandwidth efficiency.

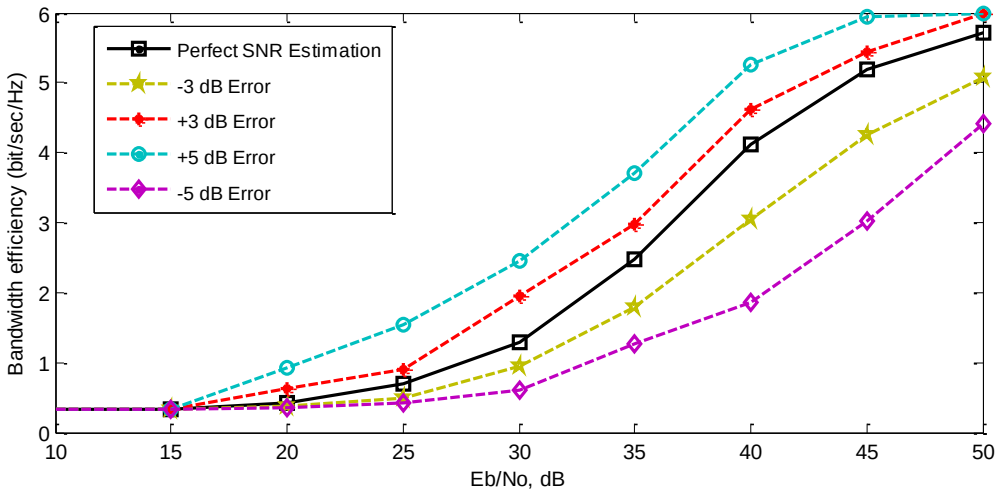

Figure 4.14: The average spectral efficiency of the adaptive modulation and channel coding scheme for target BER of 10^{-4} over Rayleigh fading channel.

A close observation of Figures 4.13 and 4.14 indicates that when the receiver overestimate the channel conditions, this may provoke the selection of a more dense constellations, leading to a higher spectral efficiency at the expense of increasing BER values. In contrast, underestimating the channel conditions, leads to less dense constellations. In this case, spectral efficiency is degraded whereas BER results are not affected so significantly. The results in Figures 4.13 and 4.14 reveal that the proposed scheme is less susceptible to imperfect channel estimation since the degradation in the average BER and the spectral efficiency is insignificant.

Chapter 5

Conclusions and Future Work

In this work, we have considered a joint adaptive modulation and channel coding scheme for wireless multimedia transmission over flat Rayleigh fading channels. We proposed a new approach that jointly considers the sensitivity of the compressed bit-stream to be transmitted and the channel state information to adapt the modulation modes and coding rates using *off-line* lookup tables. The basic idea behind the proposed scheme is to exploit the sensitivity of the compressed data to protect different portions of the multimedia stream with different channel code rates and modulation modes based upon their relative importance on reconstructed images and videos.

Based on the concept of unequal protection, we used lower modulation modes and powerful code rates for higher sensitive portions of the multimedia data and higher modulation modes and code rates for less sensitive data. An estimate of the channel condition at the receiver is fed back to the transmitter to enable selection of appropriate modulation modes and channel code rates. The adaptation attempts to maximize the bandwidth efficiency while maintaining an acceptable perceptual quality. However, the effective capacity of the channel will vary as a result of adapting the channel code rate and modulation modes, therefore the available rate for the coded source data will be dependent upon the channel conditions.

The results show that image transmission using adaptive modulation scheme achieves PSNR values that are less than those of a fixed BPSK system by 3 dB, which has a minor impact on the subjective quality of the reconstructed images. At the same time, the associated spectral efficiency is improved up to 460%. Results also demonstrate that combining adaptive modulation and channel coding for image

transmission provides a graceful trade-off between image quality and spectral efficiency. A significant improvement in the spectral efficiency was achieved over a wide range of channel states while maintaining a good perceptual quality both subjectively and objectively. When the proposed scheme was extended to wireless video transmission, an average PSNR value of 32 dB was maintained across the transmitted video frames with an acceptable perceptual quality and smooth playback. Furthermore, the robustness of the proposed scheme ensures that the overall performance degrades gracefully in the presence of imperfect channel estimation.

In future work, the performance of the proposed scheme could be analyzed when Rician channel is considered. This requires the simulation of the BER performance of the used modulation schemes and channel coding rates in Rician fading channel. The generated BER curves will be used to derive the thresholds on the estimated channel SNR to achieve a set of BERs while maximizing the bandwidth efficiency. Each time a block of data is ready for transmission, the transmitter will check the priority of the bitstream to decide the desired BER, get the estimate of the channel SNR from the receiver to compare it against the empirically derived SNR thresholds, and select the appropriate transmission parameters to be employed.

The proposed algorithm may be further extended to more complicated scenarios. For example, adaptive source coding can be incorporated with our proposed scheme. The source coder should adapt to the available channel bit rate, whereas feedback can provide a means of limiting error propagation. It is also possible to explore combining the proposed scheme with adaptive power allocation strategies to minimize the energy consumption and develop an energy-efficient scheme. Error concealment techniques may be explored as well to get a better perceptual quality.

It will be interesting to extend the developed approach by taking into consideration the video playback buffer occupancy along with the channel condition and the importance of the bit stream to reduce buffer starvation instants. This can be achieved by adapting the transmission parameters to maintain the occupancy of the playback buffer around a predefined threshold value which results in less quality vari-

ations. Adaptive playback could be employed as well to guarantee continuous video streaming. This can be done by reducing the playback rate or repeating the display of some of the frames when buffer starvation is predicted and increasing the playback rate in case of buffer overflow.

References

[1] M. Hassan and T. Landolsi, "A retransmission-based scheme for video streaming over wireless channels," *Wireless Communications and Mobile Computing*, vol. 10, pp. 511–521, Apr. 2010.

[2] M. Sabir, R. Heath, and A. Bovik, "Joint source-channel distortion modeling for MPEG-4 video," *IEEE Transactions on Image Processing*, vol. 18, pp. 90 –105, Jan. 2009.

[3] M. Hassan and M. Krunz, "Video streaming over wireless packet networks: An occupancy-based rate adaptation perspective," *IEEE Transactions on Circuits and Systems for Video Technology*, vol. 17, pp. 1017–1027, Aug. 2007.

[4] M. Sabir, H. Sheikh, J. Heath, R.W., and A. Bovik, "A joint source-channel distortion model for JPEG compressed images," *IEEE Transactions on Image Processing*, vol. 15, pp. 1349 –1364, Jun. 2006.

[5] M. Krunz and M. Hassan, "Adaptive rate control scheme for video streaming over wireless channels," in *Proceedings of the Conference on Data Compression*, pp. 242 – 251, Mar. 2004.

[6] J. Cai and C. W. Chen, "Robust joint source-channel coding for image transmission over wireless channels," *IEEE Transactions on Circuits and Systems for Video Technology*, vol. 10, pp. 962 –966, Sept. 2000.

[7] J. Lu, K. Letaief, M. Liou, and J.-I. Chuang, "Joint source and channel coding for mobile multimedia communications," in *48th IEEE Vehicular Technology Conference*, vol. 2, pp. 1224 –1228, May 1998.

[8] M. El-Iskandarani, S. Darwish, and S. Abuguba, "Reliable wireless error correction technique for secure image transmission," in *43rd Annual International Carnahan Conference on Security Technology*, pp. 184 –188, Oct. 2009.

[9] J. Wen and J. Villasenor, "Reversible variable length codes for efficient and robust image and video coding," in *Proceedings of the Data Compression Conference DCC'98*, pp. 471 –480, Mar. 1998.

[10] I. Moccagatta, S. Soudagar, J. Liang, and H. Chen, "Error-resilient coding in JPEG-2000 and MPEG-4," *IEEE Journal on Selected Areas in Communications*, vol. 18, pp. 899 –914, Jun. 2000.

[11] M. El-Tarhuni, M. Hassan, and A. B. Sediq, "A joint power allocation and adaptive channel coding scheme for image transmission over wireless channels," *International Journal of Computer Networks & Communication (IJCNC)*, vol. 2, pp. 85 – 99, May 2010.

[12] Q. Zhang, Z. Ji, W. Zhu, and Y.-Q. Zhang, "Power-minimized bit allocation for video communication over wireless channels," *IEEE Transactions on Circuits and Systems for Video Technology*, vol. 12, pp. 398 –410, Jun. 2002.

[13] M. Sabir, R. Heath, and A. Bovik, "Unequal power allocation for JPEG transmission over MIMO systems," in *Conference Record of the Thirty-Ninth Asilomar Conference on Signals, Systems and Computers*, pp. 1608 – 1612, Nov. 2005.

[14] L. Badia, N. Baldo, M. Levorato, and M. Zorzi, "A markov framework for error control techniques based on selective retransmission in video transmission over wireless channels," *IEEE Journal on Selected Areas in Communications*, vol. 28, pp. 488 –500, Apr. 2010.

[15] Y. C. Chang, S. W. Lee, and R. Komiya, "Recent advances in transport level error control techniques for wireless video transmission," in *Multimedia, Signal Processing and Communication Technologies Conference IMPACT'09*, pp. 85 – 89, Mar. 2009.

[16] D. Li, Y. Sun, and Z. Feng, "Joint power allocation and rate control for real-time video transmission over wireless systems," in *IEEE Global Telecommunications Conference GLOBECOM'05*, vol. 4, pp. 2164 –2168, Dec. 2005.

[17] D. Qiao, Y. Li, and Y. Zhang, "Adaptive modulation and power control for energy efficient video transmission over fading channels," in *2nd International Congress on Image and Signal Processing CISP '09*, pp. 1 –5, Oct. 2009.

[18] Y. Eisenberg, C. Luna, T. Pappas, R. Berry, and A. Katsaggelos, "Joint source coding and transmission power management for energy efficient wireless video communications," *IEEE Transactions on Circuits and Systems for Video Technology*, vol. 12, pp. 411 –424, Jun. 2002.

[19] C. Chi, Y. Zhang, and L. Wang, "Joint power control and FEC unequal error protection for scalable H.264 video transmission over wireless fading channels," in *IEEE Global Telecommunications Conference GLOBECOM'09*, pp. 1 – 6, Dec. 2009.

[20] Y. Q. Shi and H. Sun, *Image and Video Compression for Multimedia Engineering: Fundamentals, Algorithms, and Standards*. CRC Press, 2008.

[21] M. Ghanbari, *Video Coding: An Introduction to Standard Codecs*. Institution of Electrical Engineers, 1999.

[22] M. Ghanbari, *Standard Codecs: Image Compression to Advanced Video Coding (Telecommunications)*. Institution Electrical Engineers, 2003.

[23] A. C. Bovik, *The Essential Guide to Video Processing*. Academic Press, 2009.

[24] I. E. Richardson, *The H.264 Advanced Video Compression Standard*. Wiley Publishing, 2010.

[25] H.264/AVC JM Reference Software, Available: http://iphome.hhi.de [Accessed: May 6, 2011].

[26] C. Taylor and S. Dey, "Adaptive image compression for wireless multimedia communication," in *IEEE International Conference on Communications*, vol. 6, pp. 1925 –1929, Jun. 2001.

[27] B. Kamolrat, W. Fernando, M. Mrak, and A. Kondoz, "Joint source and channel coding for 3D video with depth image - based rendering," *IEEE Transactions on Consumer Electronics*, vol. 54, pp. 887 –894, May 2008.

[28] S. Appadwedula, D. Jones, K. Ramchandran, and I. Konzintsev, "Joint source-channel matching for a wireless communications link," in *Conference Record of the IEEE International Conference on Communications*, vol. 1, pp. 482 – 486, Jun. 1998.

[29] M. Sabir, R. Heath, and A. Bovik, "Joint source-channel distortion modelling for mpeg-4 video," in *IEEE International Conference on Acoustics, Speech and Signal Processing*, vol. 4, p. IV, May 2006.

[30] H. Y. Shutoy, D. Gunduz, E. Erkip, and Y. Wang, "Cooperative source and channel coding for wireless multimedia communications," *IEEE Journal of Selected Topics in Signal Processing*, vol. 1, pp. 295 –307, Aug. 2007.

[31] G. Baruffa, P. Micanti, and F. Frescura, "Error protection and interleaving for wireless transmission of JPEG2000 images and video," *IEEE Transactions on Image Processing*, vol. 18, pp. 346 –356, Feb. 2009.

[32] A. Al Muhit and T. C. Chuah, "Error-resilient transmission of resolution-scalable image and video over wireless channels," *IEEE Transactions on Consumer Electronics*, vol. 52, pp. 1391 –1397, Nov. 2006.

[33] E. Khan, S. Lehmann, H. Gunji, and M. Ghanbari, "Iterative error detection and correction of H.263 coded video for wireless networks," *IEEE Transactions on Circuits and Systems for Video Technology*, vol. 14, pp. 1294 – 1307, Dec. 2004.

[34] M. Torki and A. Hajshirmohammadi, "Unequal power allocation for transmission of JPEG2000 images over wireless channels," in *IEEE Global Telecommunications Conference GLOBECOM'09*, pp. 1 –6, Nov. 2009.

[35] T. Fang and L.-P. Chau, " GOP-based channel rate allocation using genetic algorithm for scalable video streaming over error-prone networks," *IEEE Transactions on Image Processing*, vol. 15, pp. 1323 –1330, Jun. 2006.

[36] T. T. Cheung, M. So, R. Cheng, and K. Letaief, "Adaptive unequal error protection and VLC reshuffling for image transmission over wireless channels," in *IEEE 51st Vehicular Technology Conference Proceedings*, vol. 2, pp. 800 –804, May 2000.

[37] S.-S. Gao and G.-F. Tu, "Robust H.263+ video transmission using partial backward decodable bit stream (PBDBS)," *IEEE Transactions on Circuits and Systems for Video Technology*, vol. 13, pp. 182 – 187, Feb. 2003.

[38] A. Goldsmith and S.-G. Chua, "Variable-rate variable-power mqam for fading channels," *IEEE Transactions on Communications*, vol. 45, pp. 1218 –1230, Oct. 1997.

[39] Z. He and W. Zeng, "Rate-distortion optimized transmission power adaptation for video streaming over wireless channels," in *IEEE International Conference on Image Processing*, pp. 3069 – 3072, Oct. 2006.

[40] J. Dani, Z. He, and X. Hongkai, "Transmission distortion modeling for wireless video communication," in *IEEE Global Telecommunications Conference GLOBECOM '05*, vol. 4, pp. 2425 –2428, Dec. 2005.

[41] Z. He, J. Cai, and C. W. Chen, "Joint source channel rate-distortion analysis for adaptive mode selection and rate control in wireless video coding," *IEEE Transactions on Circuits and Systems for Video Technology*, vol. 12, pp. 511 –523, Jun. 2002.

[42] J. K. Han and G. C. Polyzos, "Multi-resolution layered coding for real-time image transmission: architectural and error control considerations," *Real-Time Imaging*, vol. 4, pp. 275–298, Aug. 1998.

[43] I. Rhee, "Error control techniques for interactive low-bit rate video transmission over the internet," *Proceedings of the ACM SIGCOMM '98 conference on Applications, technologies, architectures, and protocols for computer communication*, vol. 28, pp. 290–301, Oct. 1998.

[44] C.-L. Wang, J.-M. Hsu, and T.-Y. Chang, "Adaptive channel estimation using the GOBA algorithm for turbo codes in rayleigh flat-fading channels," in *Proceedings of the IEEE International Symposium on Circuits and Systems*, vol. 4, pp. 45 – 48, May 2000.

[45] F. Tsuzuki and T. Ohtsuki, "Channel estimation with selective superimposed pilot sequences under fast fading environments," in *IEEE 60th Vehicular Technology Conference*, vol. 1, pp. 62 – 66, Sept. 2004.

[46] M. K. Simon and M. S. Alouini, *Digital Communication over Fading Channels: A Unified Approach to Performance Analysis*. Wiley Interscience, 2000.

[47] S. Sampei, *Applications of Digital Wireless Technologies to Global Wireless Communications*. Prentice Hall PTR, 1997.

[48] J. Proakis and M. Salehi, *Digital Communications*. Mcgraw Hill Higher Education, 2008.

[49] P. Sweeney, *Error Control Coding: From Theory to Practice*. Wiley, 2002.

[50] W. C. Huffman and V. J. Pless, *Fundamentals of Error-Correcting Codes*. Cambridge University Press, 2003.

[51] S. Lin and D. J. Costello, *Error Control Coding: Fundamentals and Applications*. Prentice Hall, 1983.

[52] B. Sklar, *Digital Communications: Fundamentals and Applications*. Prentice Hall, 2001.

[53] G. C. Clark Jr. and J. B. Cain, *Error-Correction Coding for Digital Communications*. Springer, 1981.

Appendix A

Huffman Tables for the DC and AC Coefficients of the JPEG Baseline Encoder

Table A.1: The category (CAT) of the baseline encoder [21].

CAT	Range
0	-
1	-1, 1
2	-3, -2, 2,3
3	-7,...-4, 4,...7
4	-15, ...-8, 8, ...15
5	-31, ...-16, 16,...31
6	-63, ...-32, 32, ...63
7	-127, ... -64, 64, ... 127
8	-255, ...-128, 128, ...255
9	-511,... -256, 256, ...511
10	-1023, ...-512, 512, ...1023
11	-2047,... -1024, 1024,... 2047

Table A.2: DC Huffman codewords of luminance [22].

CAT	Codeword
0	00
1	010
2	011
3	100
4	101
5	110
6	1110
7	11110
8	111110
9	1111110
10	11111110
11	111111110

Table A.3: AC Huffman codewords of luminance [22].

(RUN,CAT)	**Codeword**	**(RUN,CAT)**	**Codeword**
0, 0 (EOB)	1010	2, 5	1111111110001001
0, 1	00	2, 6	1111111110001010
0, 2	01	2, 7	1111111110001011
0, 3	100	2, 8	1111111110001100
0, 4	1011	2, 9	1111111110001101
0, 5	11010	2, 10	1111111110001110
0, 6	1111000	3, 1	111010
0, 7	11111000	3, 2	111110111
0, 8	1111110110	3, 3	111111110101
0, 9	1111111110000010	3, 4	1111111110001111
0, 10	1111111110000011	3, 5	1111111110010000
1, 1	1100	3, 6	1111111110010001
1, 2	11011	3, 7	1111111110010010
1, 3	1111001	3, 8	1111111110010011
1, 4	111110110	3, 9	1111111110010100
1, 5	11111110110	3, 10	1111111110010101
1, 6	1111111110000100	4, 1	111011
1, 7	1111111110000101	4, 2	1111111000
1, 8	1111111110000110	4, 3	1111111110010110
1, 9	1111111110000111	4, 4	1111111110010111
1, 10	1111111110001000	4, 5	1111111110011000
2, 1	11100	4, 6	1111111110011001
2, 2	11111001	4, 7	1111111110011010
2, 3	1111110111	4, 8	1111111110011011
2, 4	111111110100	4, 9	1111111110011100

table continues

(RUN,CAT)	Codeword	(RUN,CAT)	Codeword
4, 10	1111111110011101	7, 5	1111111110110000
5, 1	1111010	7, 6	1111111110110001
5, 2	11111110111	7, 7	1111111110110010
5, 3	1111111110011110	7, 8	1111111110110011
5, 4	1111111110011111	7, 9	1111111110110100
5, 5	1111111110100000	7, 10	1111111110110101
5, 6	1111111110100001	8, 1	111111000
5, 7	1111111110100010	8, 2	111111111000000
5, 8	1111111110100011	8, 3	1111111110110110
5, 9	1111111110100100	8, 4	1111111110110111
5, 10	1111111110100101	8, 5	1111111110111000
6, 1	1111011	8, 6	1111111110111001
6, 2	111111110110	8, 7	1111111110111010
6, 3	1111111110100110	8, 8	1111111110111011
6, 4	1111111110100111	8, 9	1111111110111100
6, 5	1111111110101000	8, 10	1111111110111101
6, 6	1111111110101001	9, 1	111111001
6, 7	1111111110101010	9, 2	1111111110111110
6, 8	1111111110101011	9, 3	1111111110111111
6, 9	1111111110101100	9, 4	1111111111000000
6, 10	1111111110101101	9, 5	1111111111000001
7, 1	11111010	9, 6	1111111111000010
7, 2	111111110111	9, 7	1111111111000011
7, 3	1111111110101110	9, 8	1111111111000100
7, 4	1111111110101111	9, 9	1111111111000101

table continues

(RUN,CAT)	Codeword	(RUN,CAT)	Codeword
9, 10	1111111111000110	12, 5	1111111111011100
10, 1	111111010	12, 6	1111111111011101
10, 2	1111111111000111	12, 7	1111111111011110
10, 3	1111111111001000	12, 8	1111111111011111
10, 4	1111111111001001	12, 9	1111111111100000
10, 5	1111111111001010	12, 10	1111111111100001
10, 6	1111111111001011	13, 1	11111111000
10, 7	1111111111001100	13, 2	1111111111100010
10, 8	1111111111001101	13, 3	1111111111100011
10, 9	1111111111001110	13, 4	1111111111100100
10, 10	1111111111001111	13, 5	1111111111100101
11, 1	1111111001	13, 6	1111111111100110
11, 2	1111111111010000	13, 7	1111111111100111
11, 3	1111111111010001	13, 8	1111111111101000
11, 4	1111111111010010	13, 9	1111111111101001
11, 5	1111111111010011	13, 10	1111111111101010
11, 6	1111111111010100	14, 1	1111111111101011
11, 7	1111111111010101	14, 2	1111111111101100
11, 8	1111111111010110	14, 3	1111111111101101
11, 9	1111111111010111	14, 4	1111111111101110
11, 10	1111111111011000	14, 5	1111111111101111
12, 1	1111111010	14, 6	1111111111110000
12, 2	1111111111011001	14, 7	1111111111110001
12, 3	1111111111011010	14, 8	1111111111110010
12, 4	1111111111011011	14, 9	1111111111110011

table continues

(RUN,CAT)	**Codeword**	**(RUN,CAT)**	**Codeword**
$14, 10$	1111111111110100	$15, 6$	1111111111111010
$15, 1$	1111111111110101	$15, 7$	1111111111111011
$15, 2$	1111111111110110	$15, 8$	1111111111111100
$15, 3$	1111111111110111	$15, 9$	1111111111111101
$15, 4$	1111111111111000	$15, 10$	1111111111111110
$15, 5$	1111111111111001	$15, 0(ZRL)$	11111111001

Vita

Rimas Adnan Zrae was born on January 01, 1986, in Damascus, Syrian Arab Republic. She was educated in public and private schools and graduated from Fatima Al-Zahra'a Girls High School in 2003. Then she got enrolled at Ajman University of Science and Technology Network in U.A.E, from which she graduated with merit, in 2008. Her degree was a Bachelor of Science in Electrical Engineering.

In 2009, Ms. Zrae received a graduate teaching assistantship offer to join the master's program in Electrical Engineering at the American University of Sharjah. She was awarded the Master of Science degree in Electrical Engineering in 2011. During her master's study, she co-authored two papers which were presented in international conferences.